water

MDPI

Article

Small Catchment Runoff Sensitivity to Station Density and Spatial Interpolation: Hydrological Modeling of Heavy Rainfall Using a Dense Rain Gauge Network

Clara Hohmann [1,2,*], Gottfried Kirchengast [1,2,3], Sungmin O [2,3,4], Wolfgang Rieger [5] and Ulrich Foelsche [1,2,3]

[1] Wegener Center for Climate and Global Change (WEGC), University of Graz, 8010 Graz, Austria; gottfried.kirchengast@uni-graz.at (G.K.), ulrich.foelsche@uni-graz.at (U.F.)
[2] FWF-DK Climate Change, University of Graz, 8010 Graz, Austria; sungmin.o@bgc-jena.mpg.de
[3] Institute for Geophysics, Astrophysics, and Meteorology/Institute of Physics, University of Graz, 8010 Graz, Austria
[4] Department of Biogeochemical Integration, Max Planck Institute for Biogeochemistry, 07745 Jena, Germany
[5] Bavarian Environment Agency, 86179 Augsburg, Germany; wolfgang.rieger@lfu.bayern.de
* Correspondence: clara.hohmann@uni-graz.at

Abstract: Precipitation is the most important input to hydrological models, and its spatial variability can strongly influence modeled runoff. The highly dense station network WegenerNet (0.5 stations per km²) in southeastern Austria offers the opportunity to study the sensitivity of modeled runoff to precipitation input. We performed a large set of runoff simulations (WaSiM model) using 16 subnetworks with varying station densities and two interpolation schemes (inverse distance weighting, Thiessen polygons). Six representative heavy precipitation events were analyzed, placing a focus on small subcatchments (10–30 km²) and different event durations. We found that the modeling performance generally improved when the station density was increased up to a certain resolution: a mean nearest neighbor distance of around 6 km for long-duration events and about 2.5 km for short-duration events. However, this is not always true for small subcatchments. The sufficient station density is clearly dependent on the catchment area, event type, and station distribution. When the network is very dense (mean distance < 1.7 km), any reasonable interpolation choice is suitable. Overall, the station density is much more important than the interpolation scheme. Our findings highlight the need to study extreme precipitation characteristics in combination with runoff modeling to decompose precipitation uncertainties more comprehensively.

Keywords: precipitation variability; extreme events; rain gauge network; hydrological modeling; sensitivity analysis; spatial rainfall resolution; precipitation interpolation

Citation: Hohmann, C.; Kirchengast, G.; O, S.; Rieger, W.; Foelsche, U. Small Catchment Runoff Sensitivity to Station Density and Spatial Interpolation: Hydrological Modeling of Heavy Rainfall Using a Dense Rain Gauge Network. *Water* **2021**, *13*, 1381. https://doi.org/10.3390/w13101381

Academic Editor: Scott Curtis

Received: 26 March 2021
Accepted: 11 May 2021
Published: 15 May 2021

1. Introduction

Heavy precipitation events can have significant impacts on society and ecosystems by causing severe floods and landslides. Moreover, such events are intensifying due to climate change in many areas [1–4]. Hydrological models have served as an important tool to assess the impacts of heavy precipitation events on runoff and other hydrological processes. Since precipitation is the most important input in hydrological models [5–7], it is crucial to understand its uncertainty and how this uncertainty affects the simulated runoff. Assessing the spatial and temporal heterogeneity of precipitation is becoming increasingly important, especially with respect to heavy precipitation events [8,9]. Convective storm cells with large volumes of precipitation can easily trigger hazards, but the limited spatial and temporal extent of these cells is associated with huge levels of measurement uncertainty [10]. In addition to the measurement uncertainty of rain gauges, considerable uncertainty can arise when point-level measurements are spatially interpolated

to obtain final gridded products [10–13]. Such gridded datasets are crucial in that they allow researchers to collect areal precipitation information within catchment and subcatchment areas, which can then especially be used in spatially distributed hydrological models. Areal precipitation data can also be derived from radar and satellite-based observations. However, all measurements come with their own uncertainty levels and pros and cons [7,14]. On the one hand, the point measurements are most reliable for quantitatively measuring amounts of precipitation, whereas such measurements often do not provide reliable information about the spatial patterns of heavy precipitation because of the sparse distribution of point measurement sites. On the other hand, radar systems and satellites provide higher spatial resolution data, but the indirect precipitation estimates they provide do not allow the quantitation of specific precipitation amounts [15–21].

Despite the availability of remote-sensing data, ground-based precipitation measurement tools are still widely used in hydrological modeling [6,22]. Many studies, such as those by Lopez et al. [22], Goovaerts [23], and Zeng et al. [6], pointed out the advantages of dense and regularly distributed precipitation station networks. For many years, researchers have analyzed the effect of precipitation station density on hydrological model performance [5,6,12,24–27]. Dong et al. [25] and Xu et al. [27] used a statistical approach to identify the appropriate number of precipitation gauges and the influence of gauge density on the model performance of a lumped model. Both studies found a threshold above which an increase in station density does not lead to better model performance. Such a threshold can also be seen in many other studies [5,6]. Meselhe et al. [26] applied a conceptual and a physically based model to identify the impact of temporally and spatially sampling precipitation on runoff predictions (using a highly dense station network). The physically based model was more sensitive to changes in the spatial and temporal resolution of rainfall. A threshold with no significant increase in model performance can also be seen in this case for both models. Huang et al. [12] used a lumped and a distributed hydrological model to study the sensitivity of model performance to spatial rainfall resolution. They identified temporal resolution as the most important aspect, observing better model performance at higher temporal resolutions. Many of these studies placed a focus on the model performance and used lumped hydrological models. Here, we focus on the sensitivity of runoff in small subcatchments and report results of a process-based model.

When using station data as rainfall input for hydrological models, the spatial interpolation schemes must also be considered. Many different interpolation options and possibilities have been broadly studied [28–30] including arithmetic mean [12,25,31], Thiessen polygons (TP) [6,26,32], inverse distance weighting (IDW) [13,33–35], and different types of kriging, such as ordinary kriging [8,33,35] or external drift kriging [5,27,33]. The differences between the interpolation schemes are especially pronounced when extreme values are included [30]. Therefore, the selection of interpolation schemes can affect hydrological simulations, especially under heavy rainfall events. Given that our study area has a moderate topography with regularly distributed stations [36], we did not expect to obtain added value by using more complex geostatistical methods such as kriging. Therefore, we decided to focus on the two most widely used deterministic interpolation schemes, TP and IDW. We further analyzed the weighting power parameter of the IDW interpolation, which indicates the weight of the surrounding stations. A weighting power of 2 is normally used for IDW interpolations [37] but without making any further considerations [38]. Only a few studies have analyzed the influence of the weighting power on hydrological model simulations [38,39], while some other studies have focused only on the interpolated precipitation [37,40].

To counteract the uncertainty with respect to spatial and temporal resolution, it is possible to take ground-based measurements from a highly dense station network. In this study, the following research questions were addressed: How many precipitation stations do we need to reliably model runoff during heavy rainfall events? Are there specific features of small subcatchments to reliably model runoff under heavy rainfall events? How strongly does the interpolation scheme influence runoff results when the precipitation

station density is the same? The highly dense station network WegenerNet (WEGN) (about 0.5 station per 1 km² over an area of around 300 km²) in the southeastern Alpine forelands of Austria was used to ask these questions as applied to the Raab catchment and its subcatchment areas. The region is well known for its heavy precipitation events [35,41]. Because of the exceptionally dense data coverage, it was possible to analyze the influence of precipitation station densities on runoff in detail. Therefore, we set up the widely used, physically based "Water Flow and Balance Simulation Model" WaSiM [42] and simulated runoff with varying station densities. All subnetworks were simulated using different precipitation interpolation schemes, namely, one TP scheme and three IDW schemes with a weighting power of 1 (IDW1), of 2 (IDW2), and of 3 (IDW3). Previous studies have assessed the impact of the station density and interpolation on precipitation data quality, such as mean and extreme rainfall values [43–45]. We go one step further, applying our initial study approach and focus to study the impact of such precipitation uncertainty on hydrologic simulation results, and especially on runoff peaks, using a combination of station densities and interpolation methods.

2. Study Area and Data

2.1. Study Area

The study area is part of the Raab catchment, an area of southeastern Alpine foreland draining into the Raab river. The Raab river flows from the "Passailer" Alps in the province of Styria, Austria, at an altitude of around 1150 m.a.s.l. until it joins the Danube river in Hungary. The area covered in this study ranges from the gauging station Takern II/Raab to Neumarkt/Raab, including a total area of around 500 km² (Figure 1). The gauging station Feldbach/Raab is located between these two stations. Beside the main river Raab, we analyzed five subcatchments (Table 1, Figure 1) with areas of around 10 to 30 km², all of which are covered by the WEGN. Two subcatchments are located on the northern side of the Raab and three on the southern. Since we did not have measured runoff data for these subcatchments, we implemented pour points in the model directly before they flowed into the Raab river.

The total study area is moderately hilly with elevations ranging from 230 to 530 m. The land use is predominately agricultural with some patchy forest areas. The dominant soil texture is sandy loam. The mean annual precipitation is around 850 mm, and the mean annual temperature about 9.5 °C. The study area was chosen because of its vulnerability to heavy/convective precipitation events [41] and climate change [46], as well as the data availability. Since the region has a very dense climate network, the WEGN, which is operated by the Wegener Center for Climate and Global Change, University of Graz, Austria [36]. The WEGN has been used to measure precipitation, temperature, humidity, and other variables since early 2007 and includes 150 stations within an area of around 23 × 18 km. All data are quality controlled by the WEGN QC system [36], and additional bias correction is implemented for precipitation data [47].

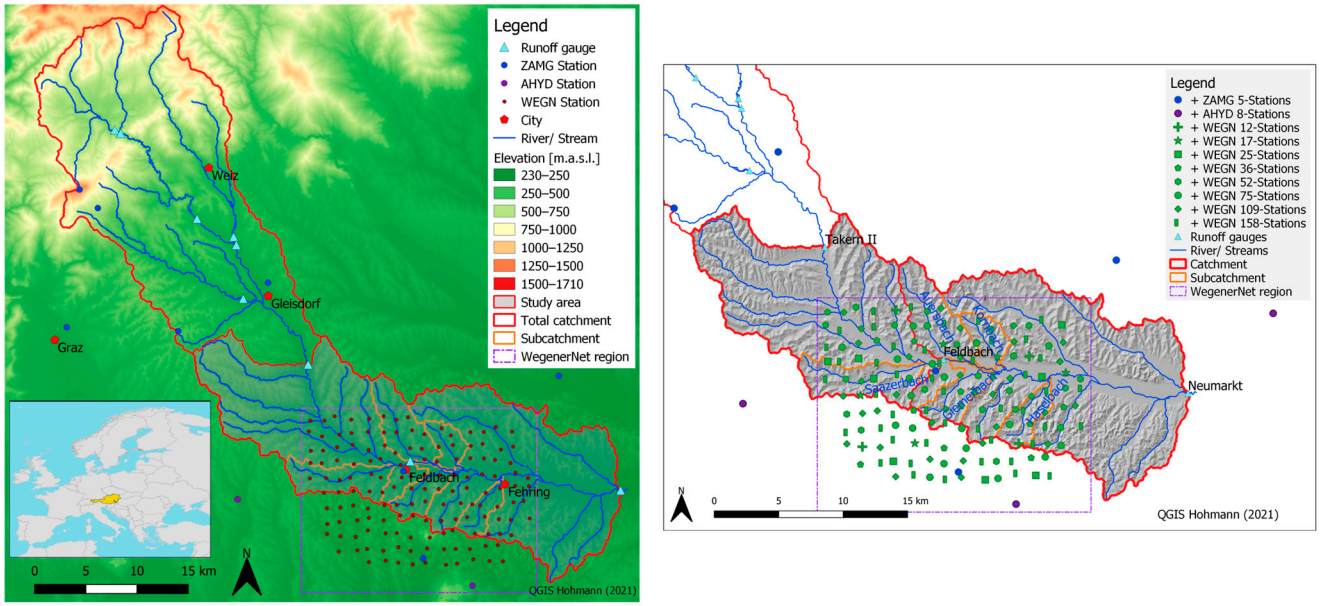

Figure 1. Map of the Raab catchment area in southeastern Austria (**left**), including the full catchment area extending down to the runoff gauge Neumarkt/Raab (red line), the focus area (grey area), the subcatchments (orange line), the WegenerNet region (violet box), the locations of rain gauge stations (dot symbols), and the runoff gauges (triangle symbols). Inset shows a map of Europe; Austria is shown in yellow and the Raab catchment, in red. An enlarged view of the study area (**right**) shows the station subnetworks and subcatchments used in this study.

Table 1. Characteristics of the study catchment area and representative subcatchment areas with the total basin area of the latter extending up to the gauging station/pour point into the river Raab.

Catchment	Area (km²)	Location from Raab
Neumarkt/Raab (total catchment)	987	-
Neumarkt/Raab (focus area)	488	-
Feldbach/Raab (total catchment)	689	-
Feldbach/Raab (focus area)	190	-
Subcatchment	**Area (km²)**	**Location from Raab**
Auersbach	28.9	north
Saazerbach	27.2	south
Giemerbach	16.0	south
Haselbach	12.3	south
Kornbach	12.2	north

2.2. Data

To perform hydrological modeling with WaSiM, we need meteorological data for precipitation, temperature, relative humidity, wind speed, global radiation, and air pressure aggregated at a 30-minute time resolution. Table 2 provides an overview of the maximum available number of stations for each parameter, as well as the station source. The WEGN has a dense station network and a 5-minute time resolution, forming a rectangular grid due to the comparability to climate models. It is located in the middle of the focus area around the Feldbach/Raab gauging station, but does not cover the total Raab catchment area. Therefore, we also needed to include data from the Austrian Weather Service (ZAMG), which has a 15-minute time resolution, and from the Austrian Hydrographic Service (AHYD), which has a 1- to 15-minute time resolution to properly simulate runoff (Table 2). In order to run the model only for the focus area, the Takern II/Raab gauging station was used as an inflow point. Runoff data from the Neumarkt/Raab gauging station were used for calibration and from the Feldbach/Raab gauging station for cross checks and further analysis. For precipitation event identification, the Integrated Nowcasting

through Comprehensive Analysis (INCA) system developed by Haiden et al. [48] was used, which is a multivariable analysis and nowcasting system developed at the ZAMG.

Table 2. Catchment attributes and hydrometeorological data used for hydrological modeling with WaSiM with the following sources: HYDROBOD—homogeneous soil and land use grids by Klebinder et al. [49]; LStmk/LBgld—state government offices of the provinces of Styria and Burgenland; TANALYS—pre-processing tool of the hydrological model WaSiM [42]; WEGN—highly dense station network data version 7.1 [50]; ZAMG—data from the Austrian Weather Service; AHYD—data from the Austrian Hydrographic Service.

Catchment Attributes	Source	Resolution
Land use types	HYDROBOD	100 m
Soil information	HYDROBOD	100 m
DEM	LStmk, LBgld	10 m
River network	LStmk, LBgld	-
Geological information	LStmk, LBgld	-
Subcatchments, slope, river width and depth, other information	TANALYS output	100 m
Meteorological Data	**Source**	**Number of Stations**
Precipitation	WEGN	150
	ZAMG	5
	AHYD	3
Temperature	WEGN	150
	ZAMG	5
	AHYD	3
Relative humidity	WEGN	150
	ZAMG	5
	AHYD	3
Wind speed	WEGN	12
	ZAMG	5
Air pressure	WEGN	1
	ZAMG	5
Global radiation	ZAMG	5
Runoff	AHYD	3

Static attributes are needed in addition to hydrometeorological station data. The digital elevation model (DEM), river network, and geological information were provided by the Austrian state government offices of Styria and Burgenland. The topographic analysis tool (TANALYS) of WaSiM uses the DEM to calculate other required grids, such as flow-time, subcatchments, slope, river width, and depth [42]. Homogeneous soil and land use grids (HYDROBOD) were provided by Klebinder et al. [49] with a resolution of 100 × 100 m in our research area. The HYDROBOD maps were created using the methods cited in Krammer et al. [51]. Maps for every single soil layer (0–20, 20–50, 50–100 cm) and parameters such as soil texture (percentage of sand, silt, and clay), saturated hydraulic conductivity, Mualem van Genuchten parameters (combinations of residual water content and saturation water content), and soil thickness were used.

3. Modeling Approach

3.1. Model Setup and Calibration

We used the hydrological model WaSiM, which was developed by Schulla [42], at the ETH Zurich in Switzerland for studying climate change in Alpine catchments. WaSiM is a well-established, widely used, distributed, and process-oriented hydrological model.

It has been used in similar catchments and for many different purposes, such as to perform climate change studies [46,52,53], land use change studies [54,55], and measure operational uses (e.g., at FOEN Switzerland). We focused on a process-oriented model to keep the model uncertainty as small as possible as compared to conceptual models, which are often used for similar precipitation runoff studies [6,12,25]. Using this type of model also allowed us to study ungauged subcatchments within our calibrated catchment area. Furthermore, WaSiM had already been successfully applied by Hohmann et al. [46] in the study area to perform a climate change sensitivity study with a low-flow focus.

In this study, we used the WaSiM-Richards Version 10.04.07. All modules of WaSiM used are shown in Figure 2. For more information about the modules, see Schulla [42] or the WaSiM user guide by Schulla [56]. The model was set up with a spatial resolution of 100 × 100 m and a temporal resolution of 30 min. WaSiM allows the option to internally interpolate the meteorological station data to grids. The evapotranspiration was estimated with the Penman–Monteith equation [57], and the unsaturated zone with the Richards equation, parameterized after van Genuchten [58]. The soil was split up into four calculation layers (0–20, 20–50, 50–100 cm, 1–20 m) with a total depth of 20 m, including the first groundwater layer. By including the data from Klebinder et al. [49], we could include a total of 416 soil parameter combinations in the soil table of WaSiM for our study domain. The final groundwater parameters of the 2D groundwater module were fitted to represent the baseflow quite accurately during the calibration period. Therefore, the saturated horizontal conductivity was split up into areas around the river with 1×10^{-3} m s^{-1} and the surrounding hilly areas with 5×10^{-4} m s^{-1}. Adopting reasonable values, the colmation factor was set to 5×10^{-5}, and the unitless specific storage coefficient to 0.2. In addition to the gridded groundwater parameters, WaSiM was calibrated using four soil module parameters, which influence the shape and volume of the simulated runoff hydrograph when no measured or literature data were available [56]: these were the storage coefficient of the surface runoff *kd* (shape of the surface runoff hydrograph) and interflow *ki* (shape of the interflow hydrograph), the drainage density for interflow *dr*, and a recession constant of the soil *krec* (both of which influence the amount of interflow).

The model calibration period was from 1 May to 30 September 2009 with a model spin-up period from 1 November 2007 to 30 April 2009. We calibrated the model only for the extended summer months (May to September), since most of the heavy rainfall events occur during these months in southeastern Styria. The validation periods were the extended summers of 2010 and 2011. The model performance was assessed with the Nash–Sutcliffe model efficiency coefficient (NSE) [59], logarithmic Nash–Sutcliffe efficiency (logNSE), Kling–Gupta efficiency (KGE) [60], and percent bias (PBIAS) [61]. NSE is the most frequently used performance measure in hydrological modelling and places a focus on peak flow [62]. To collect information about the overall flow and especially about the low-flow periods, logNSE was included [46]. KGE provides information about the correlation, bias, and variability between the simulations and observed discharge [62]. PBIAS provides the average tendency of the over- and underestimation of the discharge [61].

The calibration was mostly performed manually. To obtain a first best-guess of the model parameters, the shuffled complex evolution optimization algorithm developed at the University of Arizona (SCE-UA) [63] was used. The manual calibration was first performed with a focus on the efficiency measures and by carrying out a visual comparison of the time series of measured and simulated runoff. Second, since the runoff components such as base flow, interflow, and surface runoff are important in process-based modelling, we visually analyzed the distribution of the runoff components for specific events. Because manual calibration steps were necessary, the model was calibrated with the IDW2 interpolation and 158 precipitation stations and was not recalibrated with all different precipitation inputs and interpolation schemes. This approach is considered as appropriate, because the deviation between the efficiency measures for all studied cases from those observed in the calibration run was found to be negligible. The deviations observed in the

calibration/validation period exhibited a maximum deviation of 0.04/0.02 in NSE, 0.07/0.13 in logNSE, 0.08/0.04 in KGE, and 11/14% for PBIAS, respectively.

The best model performance was obtained with the parameter set of *krec* = 0.8, *dr* = 40, *kd* = 1.5, and *ki* = 2. This setup resulted in a model performance for the river runoff in the calibration period of summer 2009 with an NSE of 0.80, logNSE of 0.76, KGE of 0.77, and PBIAS of 8%. The validation period of summer 2010 and 2011 resulted in an NSE of 0.63, logNSE of 0.56, KGE of 0.69, and PBIAS of 19%. The observed and simulated runoff for the calibration and validation periods are plotted in Figure A2 in Appendix A.

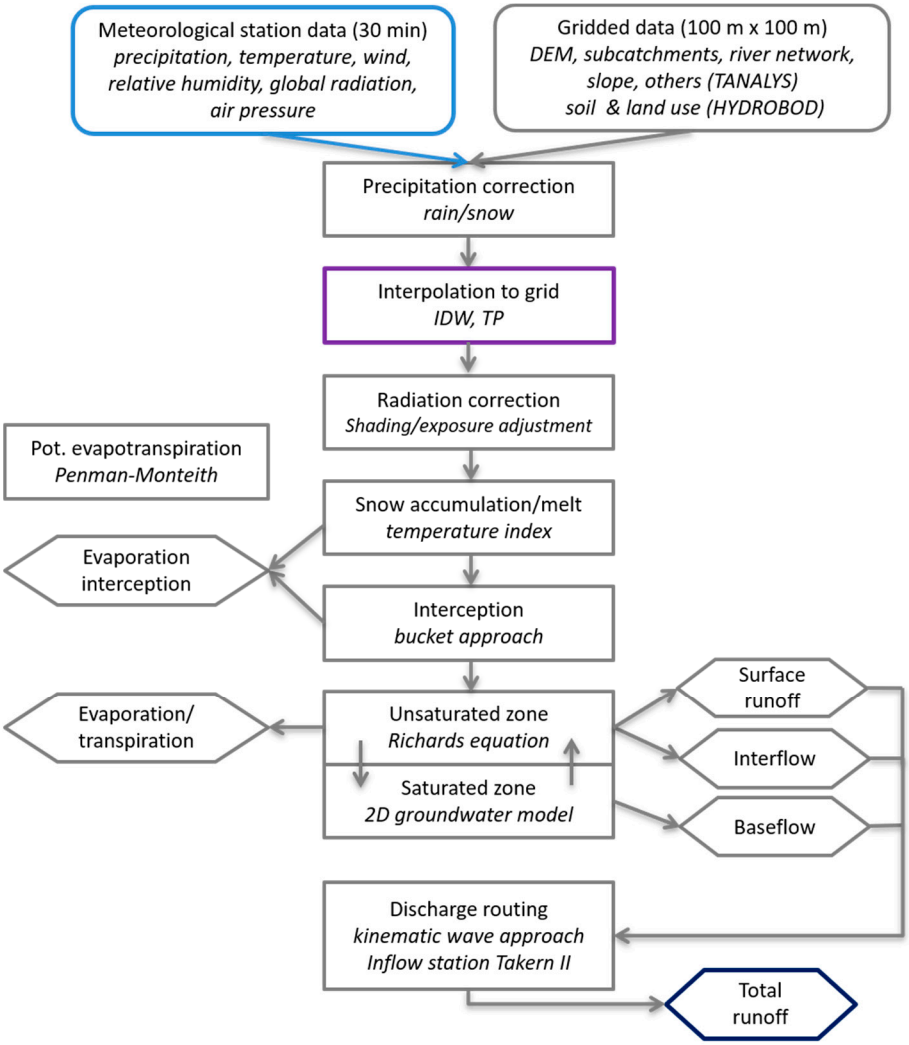

Figure 2. WaSiM model setup, including modules and input datasets used in this study (created after scheme of Schulla [56]). The focus of this study was to evaluate runoff output data (box marked in dark blue) as simulated by WaSiM with various precipitation data resolutions at input (blue box), and using different interpolation schemes (violet box) IDW—inverse distance weighting and TP—Thiessen polygons.

3.2. Experimental Design

Our study design is visualized in Figure 3 and described in the following sections.

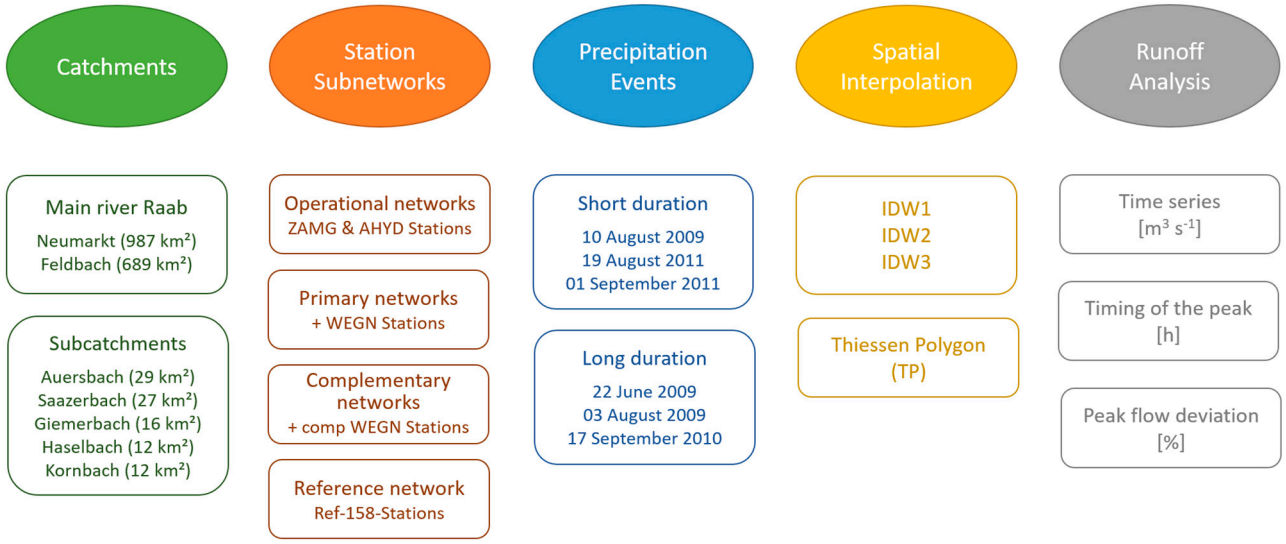

Figure 3. Overview of the study design with total catchment and subcatchment areas, gauge station subnetworks (ZAMG—data from the Austrian Weather Service; AHYD—data from the Austrian Hydrographic Service; WEGN—highly dense station network), and full precipitation network (Ref-158-Stations), analyzed short-duration and long-duration events, spatial interpolation schemes (inverse distance weighting with power of 1 (IDW1), power of 2 (IDW2) and power of 3 (IDW3); Thiessen polygons (TP)) for precipitation input data, and the key runoff output data analyzed.

3.2.1. Selection of Precipitation Station Network Densities

To obtain precipitation input data at various spatial resolutions, we defined subnetworks (Table 3 and Figure 3) using the 158 stations. The lowest-density network includes only the five ZAMG stations (5-Stations); the mean nearest neighbor distance is 11.0 km. This corresponds to an operational meteorological monitoring setup in Austria. The next subnetwork includes three more stations from the AHYD network (8-Stations). This would be a typical setup for the operational use of hydrological models.

In addition to the operational setup, precipitation stations from the WEGN are included for higher resolution subnetworks. For the main analyses, we defined seven evenly distributed subnetworks consisting of rain gauges ranging from 12–109 stations (primary subnetworks in Table 3 and Figure 1). In addition, we defined six complementary subnetwork cases ranging from 12–75 stations with different actual WEGN stations (Table 3 and Figure A1 in Appendix A). The spatial uncertainty of the precipitation depends not only on the number of gauges or station density, but also on their spatial configuration [13]. Therefore, these complementary subnetworks were considered to further investigate the uncertainty that was related to a given number of pre-defined subnetworks.

All available precipitation stations, 158 in total, served as our reference (Ref-158-Stations) with a mean nearest neighbor distance of 1.4 km. We assumed that the most accurate areal precipitation information could be obtained from Ref-158-Stations, and therefore, we calibrated the model using this setup.

Table 3. Precipitation stations of the operational subnetwork cases, the primary subnetwork cases, the complementary subnetwork cases, and the reference subnetwork with the total number of stations per subnetwork, together with the specific station data source (Z: ZAMG, A: AHYD, W: WEGN) and the estimated mean nearest neighbor distance. The distance estimates were calculated with an ArcGIS software tool.

Subnetworks	Gauge Subnetwork Case	Number of Stations (Z/A/W)	Mean Nearest Neighbor Distance (km)
Operational	5-Stations	5 (5/-/-)	11.0
	8-Stations	8 (5/3/-)	10.5
Primary	12-Stations	12 (5/3/4)	7.2
	17-Stations	17 (5/3/9)	5.9
	25-Stations	25 (5/3/17)	4.0
	36-Stations	36 (5/3/28)	3.2
	52-Stations	52 (5/3/44)	2.6
	75-Stations	75 (5/3/67)	2.0
	109-Stations	109 (5/3/101)	1.7
Complementary	12-comp-Stations	12 (5/3/4 comp)	8.3
	17-comp-Stations	17 (5/3/9 comp)	5.4
	25-comp-Stations	25 (5/3/17 comp)	4.1
	36-comp-Stations	36 (5/3/28 comp)	3.0
	52-comp-Stations	52 (5/3/44 comp)	2.4
	75-comp-Stations	75 (5/3/67 comp)	2.0
Reference	Ref-158-Stations	158 (5/3/150)	1.4

3.2.2. Selection of Precipitation Events

We selected heavy precipitation events observed with the WEGN during the extended summer (May–September) period in 2009–2014 (see also [11]). We first defined rain events with a minimum inter-event time of 6 h [64,65] and then selected the top 10% of the heaviest rainfall events. Finally, for the case studies, the three most extreme, small-scale, short-duration and the three most extreme, large-scale, long-duration events were selected (see also Figure A3 in Appendix A). The short-duration events were identified as the three events with the strongest peak hour during our study period. The long-duration events were selected as those with the largest total precipitation amount. We additionally conducted a visual inspection of the INCA data across the study area (Figure 4) to check the spatial scales of the selected rainfall events. Table 4 shows a description of the six rainfall events considered in this study.

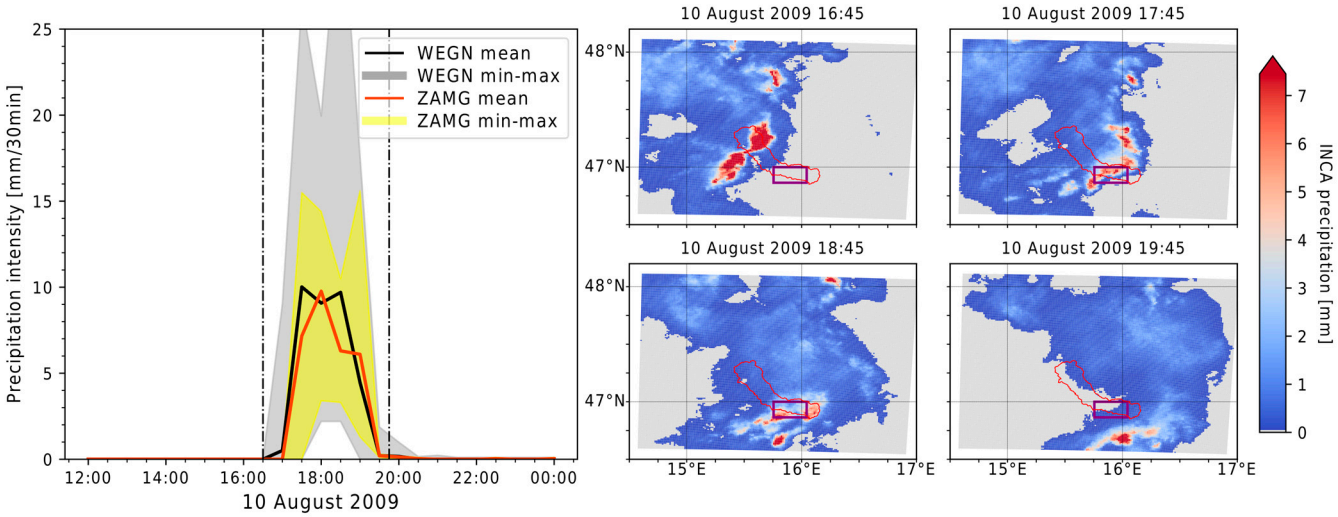

Figure 4. Precipitation time series of the "short-1 event" measured at WEGN and ZAMG stations (left panel) throughout the WEGN network area (purple box in the four panels on the right). In the panel on the left, "WEGN" shows mean areal precipitation computed from the 150 stations (black line) with a min–max range among the stations (gray shaded), while "ZAMG" shows mean precipitation (red line) obtained from the 3 ZAMG stations with a min–max range across the stations (yellow-shaded). The map sequence in the four panels on the right shows the evolution of the precipitation event as revealed by the gridded INCA analysis across the WEGN network (purple box) and the Raab catchment area (red line).

Table 4. Precipitation events selected for this study and associated key characteristics. The precipitation information indicated for the events was estimated from WEGN data. The runoff information included the measured peak runoff at the total catchment outlet, the Neumarkt/Raab gauging station. The HQ gives a rating if the peak runoff was statistically reached or exceeded once per year (HQ_1) or once per ten years (HQ_{10}).

Event	Start Date	Duration (h)	Total Precipitation (mm)	Peak Hourly Precipitation (mm)	Peak Runoff ($m^3 s^{-1}$)	HQ
short-1	10 August 2009	4	34	19	107	HQ_1
short-2	19 August 2011	2	23	18	36	$<HQ_1$
short-3	01 September 2011	4	28	26	26	$<HQ_1$
long-1	22 June 2009	66	121	10	244	$>HQ_{10}$
long-2	03 August 2009	25	106	10	213	HQ_{10}
long-3	17 September 2010	54	60	5	55	$<HQ_1$

3.2.3. Spatial Interpolation Schemes

In this work, we employed three different IDW setups and the TP interpolation. We decided to use these methods for several reasons: IDW and TP are both widely used interpolation methods in hydrological studies [30,66]. Our network is fairly dense, with regularly distributed stations in a landscape with moderate topography; therefore, we do not expect to obtain additional value from taking more complex geostatistical measures. The literature is ambiguous regarding which interpolation method is the best, and especially for high-resolution station networks, more complex geostatistical methods do not provide additional value [40,67]. The important influence of the weighting power of IDW on modeling results has not yet been studied broadly, nor has it been studied for such a dense station network [38,39]. The methods of IDW and TP are implemented in WaSiM and, therefore, widely used by the model users. Additional altitude information was not included, because the elevation differences in the area are fairly small (altitude differences are no more than about 300 m).

IDW is the sum of all contributing station data with specific weights [42]. It is calculated as follows:

$$\hat{z}(u) = \sum_j \left(w_j \cdot z(u_j)\right) \quad (1)$$

$$\text{with } w_j = \frac{1}{d(u,u_j)^p} \cdot \frac{1}{C} \text{ and } C = \sum_j \frac{1}{d(u,u_j)^p} \text{ follows } \sum_j w_j = 1 \quad (2)$$

$\hat{z}(u)$ interpolated value at location u.
w_j weight of the observed value at the station j.
$z(u_j)$ observed value at the station j.
$d(u,u_j)$ distance to the station j.
p weighting-power exponent of the inverse-distance scheme.

In our study, we used the standard weighting power p of 2 (IDW2) as well as the weighting power p of 1 (IDW1) and of 3 (IDW3) for comparison. The search radius was set differently for the core WEGN region and the surrounding stations. Since our focus region was the WEGN region itself, and we do not have such a dense network throughout the entire catchment area, we maintained a fixed precipitation input for the surrounding area. So, for the 12-Stations case and onwards, the IDW2 interpolation case with the five ZAMG and three AHYD stations and a 60 km radius of influence was maintained for the surrounding area.

The WEGN region (23 × 18 km) was then interpolated with each subnetwork and interpolation scheme, respectively. A smoothing buffer of 3 km was set, between the WEGN region and its surroundings. This setup enabled us to change the radius of influence for the WEGN stations individually without losing important information from the supporting weather stations. The radius of influence was subsequently set to 20 km for the 12- and 17-Stations cases and to 10 km for the 25-Stations case and onward so that we could include all supporting information and still obtain proper information for all locations.

Using the TP interpolation, the precipitation data collected at the nearest station were always taken. Each grid cell of the model received information from the nearest station, and the polygons formed (Thiessen polygons) represent lines of equal distance between two stations [42]. Hence, TP is a simpler method to apply than IDW, but the former is still widely used in hydrological modeling [6,26,32].

3.2.4. Runoff Analysis Approach

In our study, we analyzed an event-specific time series of runoff and peak flow deviations. The time series are visualized for all events individually, but are combined with different station network densities and interpolation schemes. For each catchment, interpolation method, and event, the peak flow deviation was calculated individually as a percent of the total value. For this purpose, the maximum runoff value was calculated using the simulation results from every subnetwork case (MAX value); this value was then compared to the maximum runoff value from the full-network reference case (MAX Ref-158-Stations), which best captures the "true" spatial variability of precipitation in the study area. This deviation metric is computed as follows:

$$\text{peak flow deviation [\%]} = \frac{(\text{MAX value}) - (\text{MAX Ref-158-Stations})}{(\text{MAX Ref-158-Stations})} \times 100 \quad (3)$$

The timing of the maximum peak flow was also calculated. Therefore, the difference between the earliest and the latest peak flows with all station densities (including the complementary subnetworks) of every single event and each catchment was calculated separately.

4. Results

4.1. Results for Individual Example Events

In this section, we focus on individual precipitation events. Figure 5 shows exemplary maps of the interpolated precipitation data, as well as the resulting runoff in the representative small subcatchment of Haselbach (12 km²) for the short-1 event. With the 12-Stations case, the maps of the two interpolation schemes and the resulting runoffs at Haselbach are very different. In the case of the Ref-158-Stations, the interpolation schemes have a smaller impact on the areal precipitation estimation as compared to the 12-Stations case. In the Haselbach subcatchment at this short-1 event, the difference between the IDW2 and TP interpolation in the 12-Stations case is more pronounced than the difference between the 12-Stations and Ref-158-Stations cases.

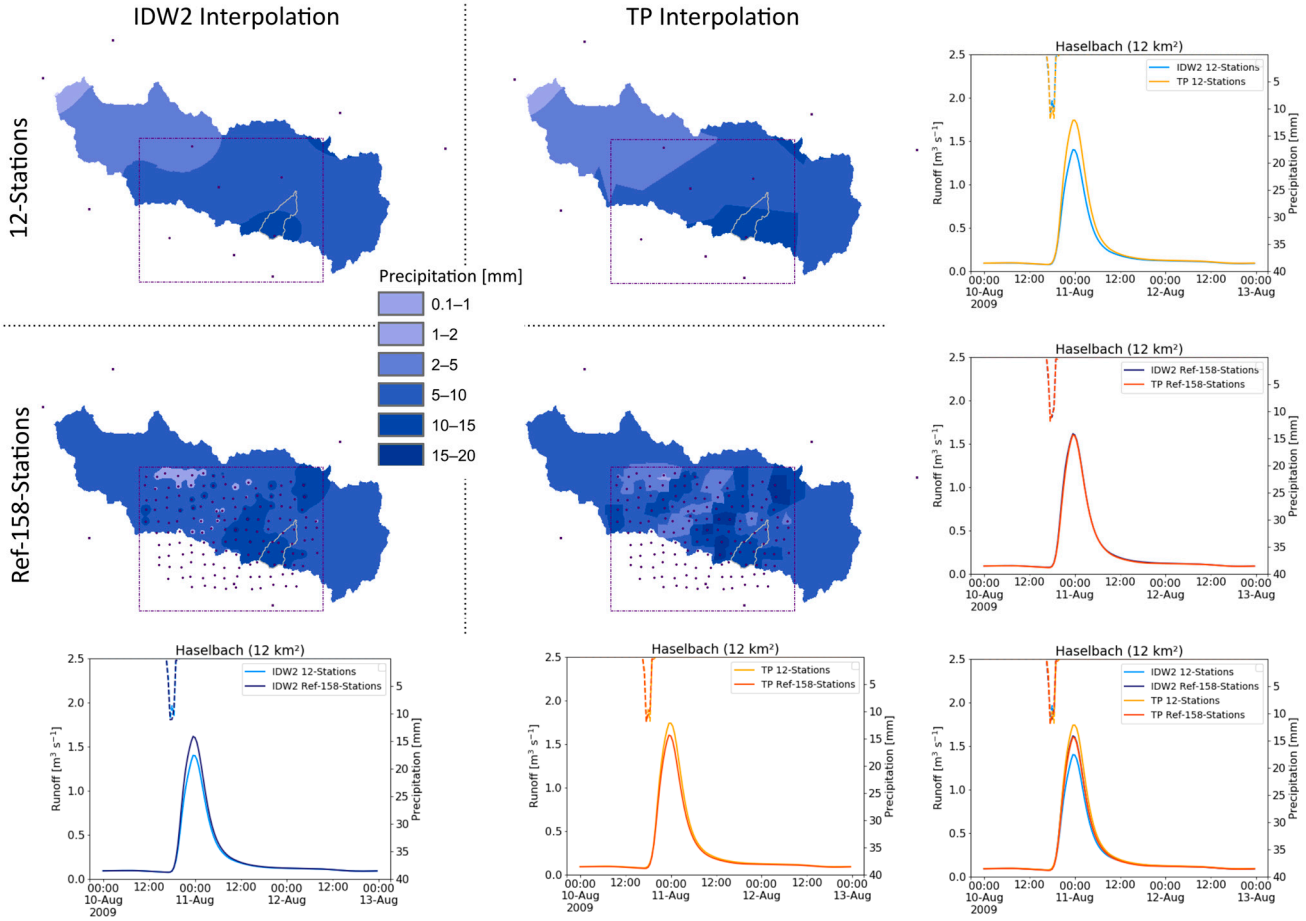

Figure 5. Exemplary precipitation maps using the WaSiM interpolation schemes of inverse distance weighting with power of 2 (IDW2) and Thiessen polygons (TP) for the short-1 event (10 August 2009 at 17:30), for the 12-Stations and Ref-158-Stations subnetwork cases (four panels on the upper-left). The time series (bottom row and right column panels) show the precipitation (dashed, from top) and the modeled runoff (solid) of this event in the representative small subcatchment of Haselbach (12 km²).

In Figure 6, the runoff time series of the short-1 event and the long-1 event for the interpolation schemes of IDW2 and TP are visualized for three subcatchments.

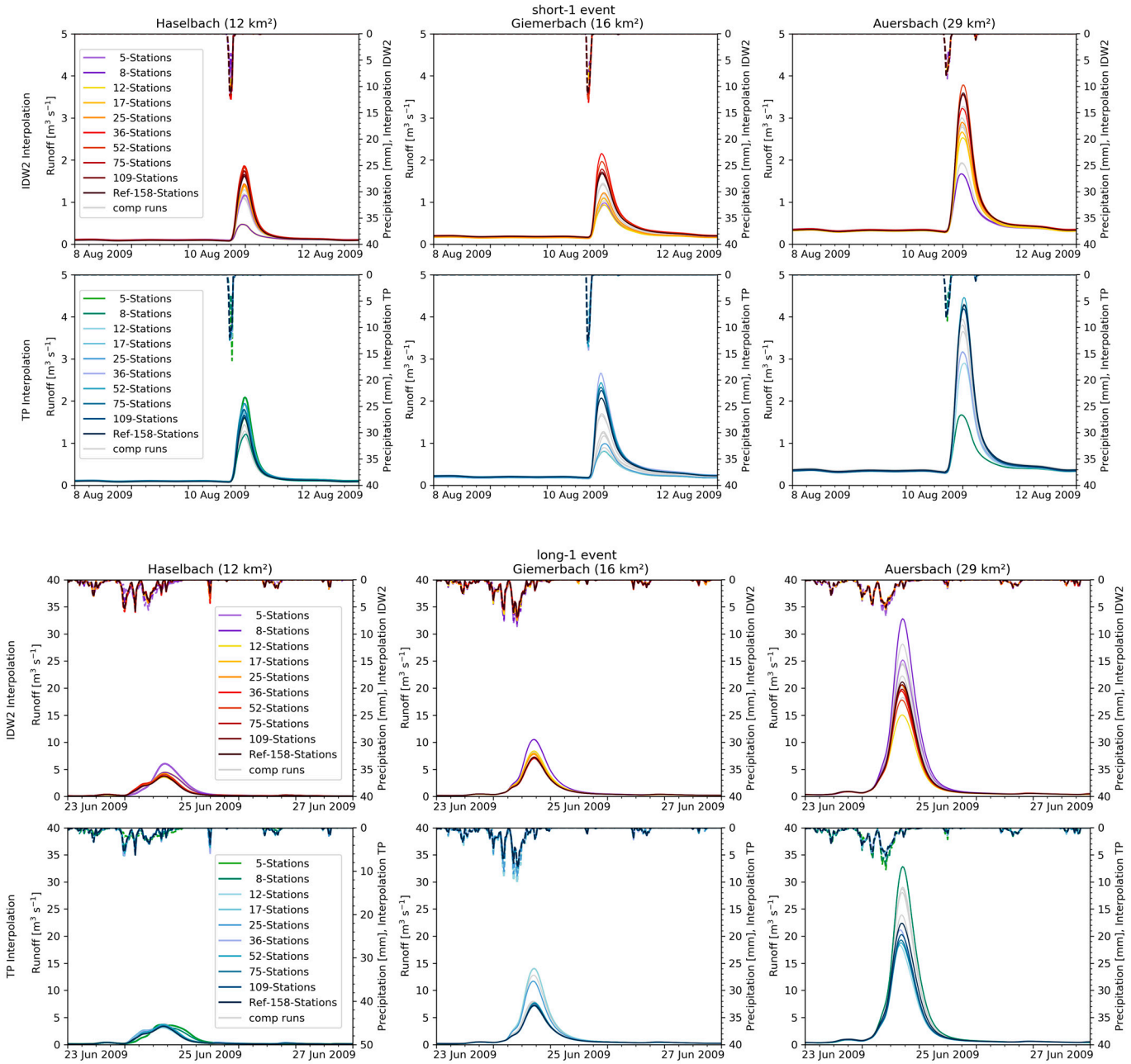

Figure 6. Precipitation and associated runoff time series for the short-1 event (top six-panel plate) and long-1 event (bottom six-panel plate), respectively, for all subnetwork cases and the full Ref-158-Stations network; the complementary runs (comp runs) for the 12-comp-Stations to 75-comp-Stations subnetworks are depicted in gray. Results are shown for the inverse distance weighting with power of 2 (IDW2) and Thiessen polygons (TP) interpolation schemes (top and bottom rows per plate), for the Haselbach (left), Giemerbach (middle), and Auersbach (right) subcatchments.

The short-1 event in the Haselbach subcatchment shows very little runoff for the 8-Stations case under the IDW2 interpolation as compared to the other cases. When examining the range of gauge densities, no systematic variation of simulated runoff peaks is observed. For instance, while the lowest runoff is simulated from 8-Stations with IDW2, the highest runoff was seen from 36-Stations with the same interpolation scheme. In the Giemerbach subcatchment, the lowest runoff is seen in the 5- and 8-Stations cases, and the

highest runoff with the 36-Stations case (both TP interpolation). Applying the IDW2 interpolation, the 36-Stations case also shows the highest value, but the 8- and 12-Stations cases show the lowest. In the Auersbach subcatchment, the IDW2 interpolation shows the lowest values with 5- and 8-Stations cases, and the highest runoff with the 52-Stations case. Applying the TP interpolation, the 5- and 8-Stations cases produce the same minimum runoff results. The maximum runoff is seen in the 52-Stations case.

The runoff results obtained for the long-1 event are almost ten times higher than that of the short-1 event. The order, maxima, and minima also differ greatly between the two. The IDW2 and TP interpolation schemes lead to a different runoff curve order and even different curve shapes. This becomes visible in the Haselbach runoff curves, which have different shapes in the two interpolation schemes and different minima and maxima. In the Giemerbach subcatchment, the highest value is simulated for the 12-Stations case with the TP interpolation and for the 5-Stations case under IDW2. In the Auersbach subcatchment, the lowest runoff is seen in the 12-Stations case with both interpolation schemes. The highest values are modelled in the 8-Stations cases when using IDW2, and in the 5- and 8-Stations cases when using TP interpolation.

These are examples of one short- and one long-duration event for three subcatchments, but they do not cover the total range of setups and results. Therefore, the combined figures are shown in Section 4.2.

4.2. Combined Results for all Events

4.2.1. Timing of Peak Flow

We calculated the differences in the timing of the runoff peak using all densities and interpolation schemes for all (sub)catchments (Table 5). The deviations range mostly between 0 and 3.5 h, with the exception of the long-3 event. The long-3 event shows huge timing differences, with up to 31 h in the Saazerbach subcatchment. Here, the first peak flow was measured on 17 September 2010 at 23:30 and the last on 19 September 2010 at 6:30. Haselbach shows a similar timing of the runoff peaks, with the exception of the 8-Stations case, when applying all interpolation schemes. In this case, the timing of the runoff peak is also one day later than in the other cases. At Neumarkt/Raab gauging station, the difference is mostly just 3 h, but the TP 8-Stations case has a maximum peak flow that is around 15 h later than the other cases.

When examining the short-1 event, we see that the runoff peaks at the Neumarkt/Raab and Feldbach/Raab gauging station were always at the same time. For the short-2 event at station Neumarkt/Raab, the timing of the peak runoff is mostly the same, but the two cases show a half-hour difference. This event also shows the smallest deviations in the peak timing, i.e., just 1.5 h. The short-3 event shows no specifically noticeable cases, whereby the timing differences at Neumarkt/Raab gauging station are up to 3 h; in the Saazerbach subcatchment up to 3.5 h; 1.5 h or less for the other catchments. When examining the long-1 and long-2 events, no specifically noticeable cases are visible, and the timing differences are just between 0.5 and 2/2.5 h.

Table 5. Calculated differences in the timing of the runoff peak for all subnetwork station densities and interpolation schemes separately for all (sub)catchments.

Event	Neumarkt/Raab	Feldbach/Raab	Kornbach	Haselbach	Saazerbach	Auersbach	Giemerbach
short-1	0 h	0 h	0.5 h	2 h	3.5 h	1 h	2 h
short-2	0.5 h	0.5 h	1.5 h	1 h	1.5 h	0.5 h	0.5 h
short-3	3 h	0.5 h	1.5 h	1.5 h	3.5 h	1 h	1.5 h
long-1	1 h	1 h	0.5 h	2 h	2 h	1.5 h	0.5 h
long-2	1.5 h	0.5 h	2.5 h	2 h	1.5 h	1 h	1 h
long-3	15.5 h	1.5 h	1 h	28.5 h	31 h	1 h	1 h

4.2.2. Peak Flow Deviation

Figure 7 shows the peak flow deviations as calculated with Equation (3) for all analyzed station cases and for the IDW and TP interpolations, respectively. The interpolation schemes of IDW1 and IDW3, as well as all results of the complementary subnetworks, are plotted in Appendix A (Figure A4). We can see that the different short- and long-duration rainfall events lead to a significantly different runoff picture, while the interpolation schemes and different catchments are much more similar. Lower station densities (<12-Stations) mostly show larger deviations from the Ref-158-Stations full network case (darker colors) than cases with more stations (lighter colors).

The three short events show more extreme differences between the station densities than the three long events. When a comparison was made between the (sub)catchments, no single (sub)catchment was especially noticeable. Using the TP interpolation generally results in more extreme values than using IDW2. Differences between the results obtained with three IDW interpolation schemes are less pronounced than differences seen between the results from IDW and TP interpolation (Figure 7 and Figure A4).

If we take a look at the short-1 event under all interpolation schemes and for all (sub)catchments, we see that the 8-Stations subnetwork shows the strongest negative peak flow deviation as compared to the Ref-158-Stations case. This sums up to nearly –70% at Saazerbach when using the IDW2 interpolation. The Saazerbach subcatchment modeling results also show slightly different behavior than the others, with a positive peak flow deviation being seen for the 5-Stations case when using the TP interpolation. Haselbach shows the most positive value of around +50% with the 36-Stations subnetwork and the IDW1 interpolation conditions.

The short-2 event reveals a similar picture as the short-1 event, with pronounced negative peak flow deviations also seen for the less dense networks. Again, the most negative deviation appears in the Saazerbach subcatchment in the 8-Stations case (IDW2) with nearly –65%. The most positive values are obtained when TP interpolation is used for the Saazerbach, Giemerbach, and Haselbach subcatchments.

The short-3 event shows a more positive peak flow deviation pattern as compared to those obtained in the short-1 and short-2 events. Especially Auersbach shows positive deviations, with more simulated runoff seen than in the Ref-158-Stations cases for almost all interpolations and station density cases. Including data from the complementary network, but also the primary networks, results in quite extreme values for the short-3 event. The runoff gauges at the main river stations of Neumarkt/Raab and Feldbach/Raab seem to reflect the mix of extreme positive and extreme negative peak flow deviations with maximum values of around +15% and −30%.

The long-1 event shows the strongest peak flow deviations among the long duration events. Giemerbach shows especially high positive values when TP interpolation is used, deviating from the Ref-158-Stations case by up to 90%. Auersbach shows different behavior, with the most negative values observed for the 12- to 52-Stations cases and deviations of up to –35%. The 5- and 8-Stations cases result in positive peak flow deviations in all catchments.

The long-2 event shows less pronounced peak flow deviations than the long-1 event. Haselbach and Kornbach show the most positive deviations with up to +60% seen in the 5- and 8-Stations cases.

The long-3 event appears to be very similar to the long-2 event, showing little peak flow deviations in most of the cases. Here, Saazerbach shows the most positive peak flow deviation in the 8-Stations case when TP interpolation is used, i.e., +75%.

By comparing all events together, some results can be summarized for individual (sub)catchments. For the Raab river gauging stations of Feldbach/Raab and Neumarkt/Raab, the peak flow deviation starting from the 25-Stations subnetwork is almost the same as the Ref-158-Stations full network (less than 10%). This implies that data from the 25-Stations network would be sufficient to adequately simulate the Raab river runoff. However, the complementary network shows deviations of up to 14% for the gauge at

Neumarkt/Raab in the 25-Stations case, and here, using only the 36-comp-Stations case would be sufficient, as it shows deviations below 10%. At the Feldbach/Raab gauging station, using the 36-Stations case of the primary subnetwork results in deviations below 10%, but using only the complementary subnetwork is not sufficient, even with 75-comp-Stations.

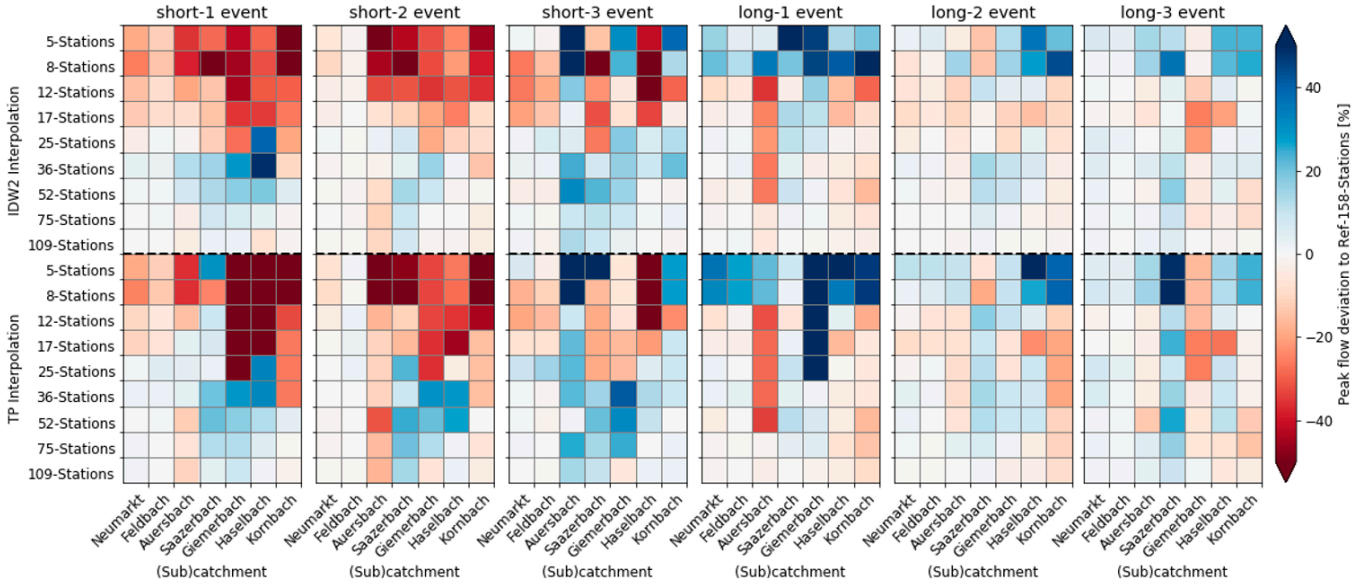

Figure 7. Peak flow deviation from the Ref-158-Stations case as a grid-cell plot with each cell indicating the magnitude of the deviation on a color scale. The cases of all six events (one event per panel), all (sub)catchments (columns within each panel), two interpolation schemes IDW2—inverse distance weighting with power of 2 and TP—Thiessen polygons (stacked subpanels in each panel), and all subnetwork cases (rows per subpanel) are shown.

Auersbach and Saazerbach show a deviation of more than 10% at least for one event, where even the 109-Stations case does not result in the same runoff as the 158-Ref-Stations case. Giemerbach and Kornbach show a threshold at the 109-Stations case, after which no large improvement in the accuracy of the simulated runoff is seen, compared to the Ref-158-Stations case. Haselbach already shows such a threshold in the 75-Stations case.

On the one hand, the inclusion of data from a specific number of stations leads to large changes in simulated runoff in many subcatchments. Giemerbach shows such a large step/change from the 25- to the 36-Stations case (e.g., in the short-1 event when using the TP interpolation, the value for the 25-Stations case is around −50%, and for the 36-Stations case +30%). These large steps are especially noticeable for the short-duration events, but are also measurable for the long-duration ones. The Haselbach subcatchment also shows this behavior, but between the 17- and 25-Stations cases.

On the other hand, no changes between some subnetworks are visible in some subcatchments, especially when using the TP interpolation. The northern catchments Auersbach and Kornbach almost do not show differences if we simulate runoff using data from 5- or 8-Stations subnetworks and all interpolation schemes (<1%). If we use the TP interpolation, the analysis of data from the 17-, 25-, and 36-Stations subnetworks lead to the same peak flow results in these northern catchments. Giemerbach shows almost the same runoff in all events in the 5-, 8-, and 12-Stations, and also between the 17- and 25-Stations cases.

In Figure 8, we summarize the results for peak flow deviations as a function of all station subnetworks for the primary and the complementary subnetworks. These results highlight the fact that the direction of biases (overestimation vs. underestimation) is affected primarily by the gauge network density rather than the interpolation scheme used. For long-duration heavy precipitation events, assessing a mean value over all catchments, we find that the biases decrease more rapidly when the number of gauges in the network

increases. The long-duration heavy precipitation events as a mean over all (sub)networks show a threshold behavior with 17 regularly distributed stations, yielding satisfactory performance for all interpolation schemes. From the 17-Stations case and onward, the bias is less than about 10% and converges with higher subnetwork densities.

Note that our subnetworks represent a quite regularly distributed gauge configuration, and therefore, the uncertainty in the runoff simulations can be somewhat greater than for more irregular gauge location configurations, which is visible in the complementary station case. Here, the 25-comp-Stations case would be sufficient, after which no large improvement in the runoff accuracy compared to the Ref-158-Stations case becomes visible.

The short-duration heavy precipitation events show such a threshold behavior in the 52-Stations case, within the 10% range. Above this threshold, the values converge with higher subnetwork densities. In the complementary network, 75-comp-Stations are also below the 10% deviation, so this case would be as good as the Ref-158-Stations case if data are averaged across all (sub)catchments.

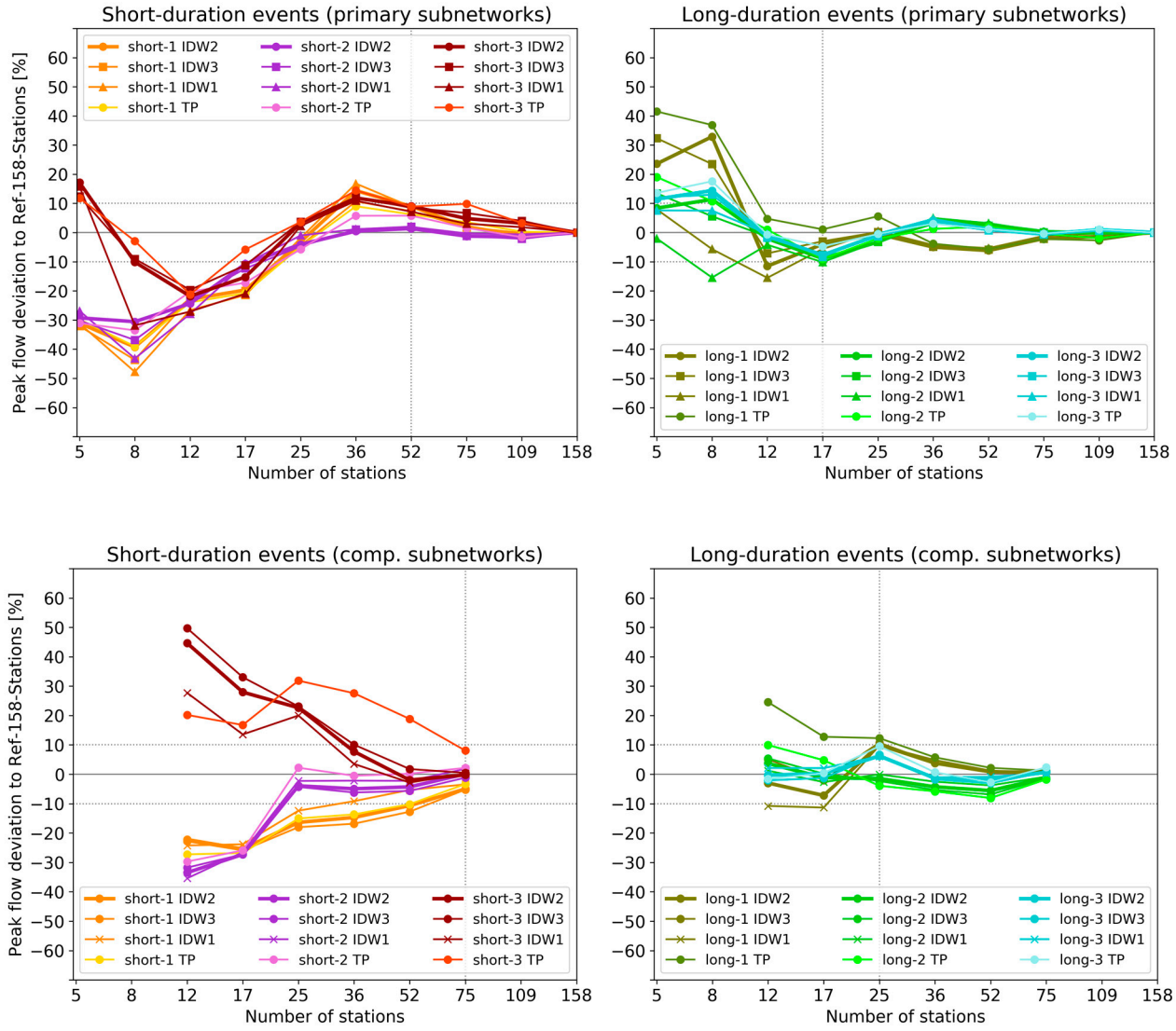

Figure 8. Peak flow deviation between the Ref-158-Stations case and the mean across all (sub)catchments for all subnetwork cases (*x*-axis of panels) and interpolation schemes (different line styles, see legend) IDW2, IDW3, and IDW1—inverse distance weighting with powers of 2, 3, and 1, TP—Thiessen polygons, respectively, for the three short events (**left**) and the three long events (**right**). The data shown in the upper panels were calculated based on the ten primary subnetwork cases (5- to 158-Stations) and in the lower panels, for the six complementary ones (12-comp- to 75-comp-Stations).

5. Discussion

In our event-based study, we chose the three most extreme short- and long-duration events. Significant differences in peak runoff among these six events were observed at the Neumarkt/Raab gauging station, in part due to different preconditions: the short-1 event, with over 100 $m^3 s^{-1}$ peak flow, was influenced by the long-2 event that had occurred a few days before, and the other two short events in 2011 had drier preconditions and consequently smaller peak flows with 26 to 36 $m^3 s^{-1}$.

5.1. Threshold Behavior

The mean over all catchments and events (Figure 8) shows a "sufficiency threshold"; above this density, only small runoff changes of about 10% can be observed, which converge when higher subnetwork densities are used. For the long-duration events, this threshold occurs in the 17-Stations case using a regularly distributed subnetwork. This corresponds to a mean nearest neighbor distance of 5.9 km or around 30 stations per 1000 km^2. The short-duration events only show such threshold when the 52-Stations case is analyzed using the primary subnetwork (mean distance of around 2.6 km or around 150 stations per 1000 km^2). Such thresholds have also been reported in the literature, where no better performances after crossing specific station densities are seen [5,22,25,27]. For example, Lopez et al. [22] mentioned a threshold of 24 gauges per 1000 km^2 for the Thur basin (area 1700 km^2), and Xu et al. [27] of around 1 rain gauge per 1000 km^2 for the Xiangjiang River catchment (area 94,660 km^2). Evidently these studies focused on large catchments and larger scales. By comparing the results of the primary network with the results obtained from the complementary networks (i.e., irregularly distributed stations), we found that collecting data from a regularly distributed network requires the use of fewer stations to properly simulate runoff.

In contrast to these "sufficiency thresholds", the individually fairly small subcatchments do not always show such a sufficient density in our high-resolution case, where the results are both catchment- and event-dependent (Figure 7). Compared to the Ref-158-Stations cases, a sufficient density can only be reached in the Giemerbach and Kornbach subcatchments using a high density with the 109-Stations. In the Auersbach and Saazerbach subcatchments, this is not possible even with 109-Stations. In the Haselbach subcatchment, using the 75 stations of the primary subnetwork are sufficient, but not using the 75 complementary stations. For this, a much denser and well-targeted network is needed to obtain peak flow deviations that are lower than 10% as compared to the Ref-158-Stations case in small subcatchments.

5.2. Influence of Station Location

Adding four WEGN stations to the operational subnetworks (5- and 8-Stations cases), we noticed that including data from the first four WEGN stations in the primary subnetwork (12-Stations cases) consistently resulted in much lower peak flow deviations from the Ref-158-Stations case, but including data from the first four complementary stations (12-comp-Stations) led to much higher peak flow deviations. Therefore, in catchments where station numbers are still sparse, the location of the stations is very important for mitigating the under-sampling problem. Watson et al. [62] pointed out that not only the density of precipitation measurements has a significant impact, but also that the stations needed to be positioned in critical areas.

The effect of the station location is clear within the operational setup when comparing the 5- and 8-Stations cases. In the Auersbach and Kornbach subcatchments, the peak flow under all interpolation schemes in these cases is the same for subcatchments on the northern side of the Raab river. These two catchments are not influenced by the AHYD stations located to the west, south, and farther east of the Raab river. However, the precipitation input of the Saazerbach subcatchment is often strongly influenced by AHYD

stations to the west of the river that supply meteorological information. This information is especially important, since many storms come into the area from the west or north-west.

In some cases, the simulated runoff did not change, even when more stations were included. Using TP interpolation in Giemerbach, Kornbach, and Auerbach subcatchments, it did not matter whether we used 5-, 8-, or 12-Stations or the 17- and 25-Stations case. The peak flow deviation always stayed the same for the primary subnetwork, because the supporting stations are too far away to be included when using the TP interpolation. These effects were not as pronounced when IDW interpolation schemes were used, since the influence radius here also included information from weather stations that are within the larger surrounding area.

Due to the "right" location change, the simulated runoff differed strongly from one subnetwork to the other in some cases. In the Haselbach subcatchment in the 17- to the 25-Stations case (IDW2), a change of around −30 to +40% peak flow deviation occurred. This is because one WEGN station of the 25-Stations case is very close to the subcatchment. In the Giemerbach subcatchment, changes from −50 to +30% were observed (25- to 36-Stations case), because two WEGN stations were added, and these are located directly in the catchment. Therefore, we observed that the location of the gauging stations is highly crucial in areas where the sampling densities are basically still insufficient.

By placing our focus on small catchments, we can clearly point out that the station density has a larger influence on small subcatchments than on the total Raab catchment. The specific spatial location of precipitation stations is much more important when analyzing data for small catchments. It has already been noted in other studies that the location of precipitation measurements is important on all scales [22,24,68]. Using the highly dense WEGN, we could show new empirical evidence that again underlines the importance of these locations in small catchments, i.e., in the 10 to 30 km^2 area class.

5.3. Effect of Timing of Peak Flow

By analyzing the timing of peak flow (Table 5), we see that the differences are mostly quite small as compared to the model time resolution of 30 min. Nevertheless, a difference of three hours can make substantial difference regarding (flash) flood prevention, especially in small catchments. This difference is most profound when the time difference arises only from the station network density in combination with the station locations. In the special case of the long-3 event with a precipitation event duration of 54 h, the absolute peak runoff occurs even on different days. The total rainfall of 60 mm fell over a long time period, and depending on the station density and location, different amounts were simulated in the area. This result is especially important with respect to small catchments, where the influence of specific stations is even more pronounced. As seen before, the total Raab catchment at station Neumarkt/Raab is also influenced by this effect, and a time difference up to 9 h can occur.

5.4. Comparison of Interpolation Schemes IDW and TP

Turning specifically to examine the characteristic influences of the interpolation scheme, several aspects are salient, including the special properties of TP interpolation. Precipitation maps of interpolated gridded rainfall are generally very different when different IDW and TP interpolations are used with stiff borders between the TP polygons (Figure 5). These lead to sharp differences in simulated precipitation amounts between two adjacent polygons, especially in cases of high spatial rainfall variability. Therefore, the greatly pronounced peak flow deviation is also due to this reason (Figure 7).

Compared to using the different IDW interpolation schemes, the effect of using the TP interpolation is much stronger. However, by comparing the three IDW interpolation schemes, we see that the differences among them are not negligible. Peak flow deviations of up to 50% from the IDW2 to the IDW1 case are possible (e.g., short-3 event, 5-Stations, Saazerbach). The influence of the interpolation scheme is highly event-dependent and especially pronounced in small catchments with a low subnetwork number. For the total

catchment area of Neumarkt/Raab and Feldbach/Raab, the differences are below a 5% deviation. In this case, it does not make a difference which IDW scheme is used, but the choice between IDW and TP is distinct.

Among the IDW interpolation schemes, the peak flow deviations of IDW3 tend to be the closest ones yielded by using the TP interpolation. This result is expected, since the higher IDW3 weighting power gives less weight to the surrounding stations than IDW2 or IDW1. Dirks et al. [40] suggested using the power values of 2 for daily and monthly, 3 for hourly, and 1 for yearly precipitation interpolations to minimize the interpolation error. Kurtzman et al. [39] mentioned that the influence of weighting power depended on spatial pattern, specifically referring to the location of the catchment in their Mediterranean study area. Large power values of 3 are more effective closer to the coast line, whereas smaller power values such as 1 are more effective closer to the mountains. Our study area is close to the mountains, which seems to support the observations of Kurtzman et al. [39] regarding the IDW1 interpolation, but we use half-hourly time steps, which is more similar to the use of the IDW3 method in Dirks et al. [40]. Our results do not suggest that there is a certain IDW weighting power value for performing optimal hydrological modelling in the Rabb catchment. We used the IDW2 as reference, as it is also the most widely used [37]. In other studies in the WEGN region, the weighting power of 2 was also set for the precipitation interpolation [69,70] based on performance tests such as leave-one-station-out verifications on small-scale rainfall events. Nevertheless, if we use many stations, we see no relevant difference between the different weighting power of the IDW interpolations from about from the 52-Stations case onward (mean distance of around 2.5 km).

Overall, if only a few stations are available, the IDW interpolations, and in particular IDW2, are preferable for analyzing data from regions with moderate topography. The TP interpolation is not recommended for areas with complex topography and low station densities, as also stated by Kobold and Brilly [32]. Dirks et al. [40] also do not recommend the TP interpolation, because of its unrealistic discontinuous rain fields, although the interpolation errors between TP and IDW are comparable. Only when the network is highly dense, as in our cases with at least 350 station per 1000 km^2 or more, the TP method might be an option, since it is computationally the least expensive. Nevertheless, precipitation maps with sharp differences that are still unrealistic will exist that could adversely impact runoff results in very small catchments.

In summary, our results clearly show the influence of the interpolation scheme on modelling, especially for few-station networks. Nonetheless, the impact of station network density is clearly much more significant for runoff simulations than the impact of the interpolation scheme.

6. Conclusions

We used the highly dense WEGN station network in the southeastern Alpine foreland of Styria, Austria, to analyze the influence of rain gauge network density and interpolation schemes on simulated runoff, placing a focus on small subcatchments (10 to 30 km^2).

Our first key question was "How many precipitation stations do we need to reliably model runoff during heavy rainfall events?" This question cannot be answered in general due to the complex spatiotemporal characteristics of the events, and especially of the short-duration convective events. Although our results show that the influence of the station network density is specifically catchment-, (station) location-, and event-dependent, we were able to derive average, guideline results.

For long-duration stratiform-type events (lasting typically longer than a day) and averaging over all catchments, a station density with a mean nearest neighbor distance of around 6 km (17-Stations) is found to be sufficiently dense to perform robust runoff modeling, including reliable peak runoff estimations. To obtain an average for all catchments from the short-duration heavy convective rainfall events (lasting typically a few hours only), at least a mean nearest neighbor distance of around 2.6 km (52-Stations, regularly distributed subnetwork) is needed for runoff modeling. Our simulations with data from

the complementary subnetworks show that not only the density of stations but also their spatial configuration is crucial.

The second research question "Are there specific features of small subcatchments to reliably model runoff under heavy rainfall events?" can be answered with a clear "Yes". By focusing on subcatchments in the 10 km^2 size class, our results show that sufficient station density is mostly higher with 109-Stations (mean distance 1.7 km) or not even reached at numbers lower than the reference case. Therefore, especially in small subcatchments, both the station density and the actual station locations are crucial. Here, the influence of station location also depends on typical storm tracks across the catchment.

Furthermore, the radius of influence of each station plays an important role for precipitation interpolations. The third key research question "How strongly does the interpolation scheme influence runoff results when the precipitation station density is the same?" is related to this. The answer to this question depends on the station density. For very dense station networks (in our case 109 to 158 stations, mean distance of 1.7 km to 1.4 km), the specific interpolation scheme is not relevant. The simpler TP interpolation is already sufficient in these cases, although it can provide unrealistic rainfall fields. Overall, the interpolation scheme is found to be clearly less influential than the gauge network density on simulated runoff. Hence, when analyzing and interpreting modeled runoff based on rainfall input data, station network density will most importantly influence the results as long as a reasonable interpolation is chosen.

We emphasize that it is important to carry out an explicit study of the hydrological response to different precipitation events. Many earlier studies have evaluated the "accuracy" of (remote-sensing) gridded rainfall event data by making direct comparison with ground gauge measurements [18,19,71]. Our study findings highlight the fact that it is also important to evaluate the performance of precipitation datasets at various resolutions to measure hydrological runoff response. Such evaluations will provide broader practical guidance both to rainfall data providers as well as to hydrological model users.

The dependence on specific rainfall event characteristics and station network density is mitigated in the main river runoff. However, regarding local-scale hazards that can occur, such as severe overland flooding, flashfloods, and hillslope landslides that are triggered by short-duration convective events, it is necessary to obtain more dense observations to perform reliable hydrological modeling and estimate the risks of these hazards and suggest protective action. While the WEGN is a unique, long-term research facility with sufficiently high station density, it is quite limited in terms of area. The densification and expansion of runoff and rainfall gauge networks in this and many other risk-prone areas, therefore, would be a great and much needed improvement on top of existing observations. An alternative would be to tap other data sources, enabling suitable data products to be obtained at high spatiotemporal resolutions, such as well-calibrated, high-quality precipitation radar data.

In deploying new stations, selected station locations have a strong effect on gridded precipitation fields and, therefore, also on runoff results, especially in small catchments. In this study, we selected two subnetwork ensembles, the primary and the complementary subnetwork with gauges from the WEGN. The primary subnetwork contained stations with a quite regular distribution, and the complementary subnetwork contained different WEGN stations. Performing a more detailed analysis, whereby the influences of irregular distributions are examined by randomly picking and evaluating stations more closely on the basis of catchment characteristics, may be a useful design step for determining new station placements in other areas. This would help us to arrive at an optimal rain gauge network design for hydrological purposes in the specific catchment.

Since such dense networks are available in virtually no other place worldwide, the runoff impact results derived here for the Raab catchment and its subcatchments in southeastern Austria need to be "transferred" to other regions with due care, examining the comparability of weather, hydrology, and landscape characteristics [36,41,72]. With such due care, we consider the essential results and conclusions to be transferable to many

other mid-latitude land regions. For the majority of ungauged or extremely sparsely observed small catchments, the awareness of both the level of skill and limitations of rainfall–runoff modeling, as reported here, will be particularly crucial.

Author Contributions: All authors designed the study, with primary contributions by C.H. and G.K. C.H. collected the data, performed the modeling and most of the analysis, created the figures, and wrote the first draft of the manuscript. G.K. provided guidance and advice on all aspects of the study and significantly contributed to the figure design and the text. S.O. contributed to the data collection, precipitation data analysis, and figure creation. W.R. supported the model calibration and validation. All authors helped to shape the research and analysis; they provided critical feedback and contributions to the text until submission and during review. All authors have read and agreed to the published version of the manuscript.

Funding: This research has been supported by the Austrian Science Fund (FWF) Doctoral Programme Climate Change—Uncertainties, Thresholds and Coping Strategies (grant no. W1256) and the University of Graz.

Institutional Review Board Statement: Not applicable.

Informed Consent Statement: Not applicable.

Data Availability Statement: The hydrological model WaSiM is available via http://wasim.ch (accessed on 25 March 2021) (version used: WaSiM-Richards 10.04.07). The WegenerNet data are available at https://doi.org/10.25364/WEGC/WPS7.1:2021.1 (Fuchsberger et al. [50]: WegenerNet climate station network Level 2 data version 7.1 (2007–2020); Wegener Center, Univ. of Graz, Austria). ZAMG data are available from the Austrian Weather Service (www.zamg.ac.at, accessed on 25 March 2021) and AHYD data from the Austrian Hydrographic Service (https://ehyd.gv.at, accessed on 25 March 2021). HYDROBOD data are used from Klebinder et al. [49] and are available on request from these authors. Geoinformation data are from state government offices of Styria and Burgenland and are available from the respective GIS services (www.gis.steiermark.at; https://geodaten.bgld.gv.at, accessed on 25 March 2021).

Acknowledgments: The authors thank J. Fuchsberger (Wegener Center, Univ. of Graz) for support and advice on the WegenerNet data, S. Birk (Inst. for Earth Sciences, Univ. of Graz) for discussions and advice on the water balance and groundwater characteristics of the catchment, and V. Hess (DK Climate Change, Univ. of Graz) for several fruitful discussions and support during the study work. We also thank the anonymous reviewers for their helpful comments. Furthermore, we acknowledge the data providers at the Austrian Weather Service (ZAMG), the Austrian Hydrographic Service (AHYD), the state government offices of Styria and Burgenland, and the Wegener Center regarding the WegenerNet data. WegenerNet funding is provided by the Austrian Ministry for Science and Research, the University of Graz, the Styrian Provincial Government (which also included European Union regional development funds), and the city of Graz; detailed information can be found online (www.wegcenter.at/wegenernet, last access: 25 March 2021). This research project has been funded by the Austrian Science Fund (FWF) Doctoral Programme Climate Change—Uncertainties, Thresholds and Coping Strategies (grant no. W1256) and the University of Graz. Open Access Funding by the Austrian Science Fund (FWF).

Conflicts of Interest: The authors declare no conflict of interest.

Appendix A

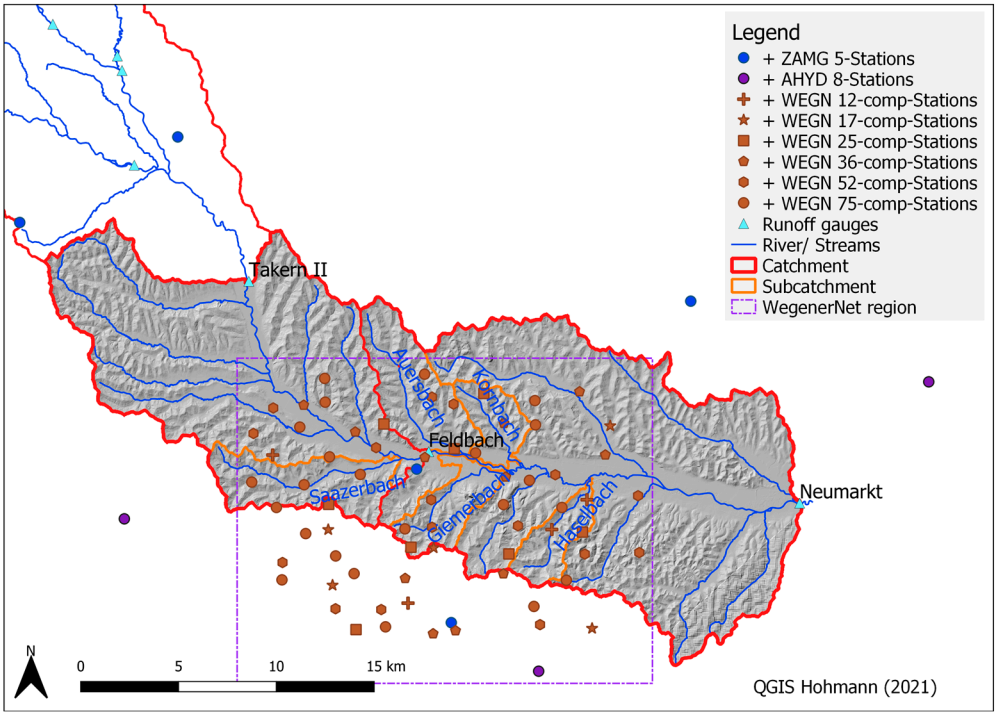

Figure A1. Enlarged view of the study area, as in Figure 1, indicating the complementary subnetwork setups and subcatchments used in the study.

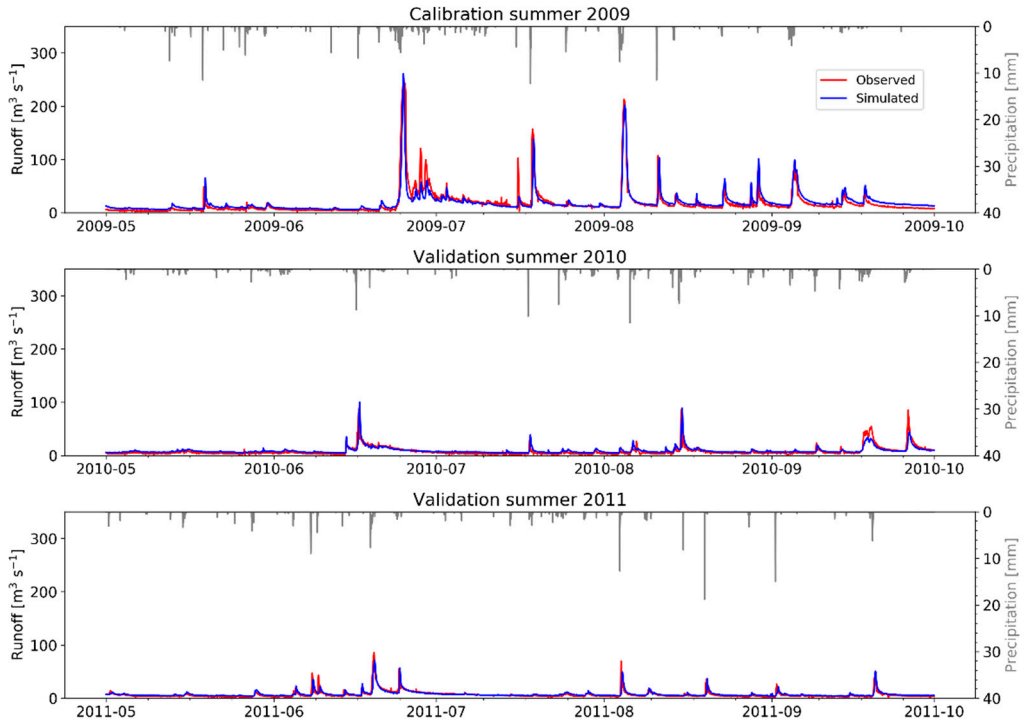

Figure A2. Simulated (blue line) and observed runoff (red line) at the Neumarkt/Raab gauging station for the calibration period of May to September 2009 (top) and the validation period of May to September 2010 (middle) and 2011 (bottom). From the top of each panel, the interpolated precipitation (grey line) is co-visualized over the same extended summer periods.

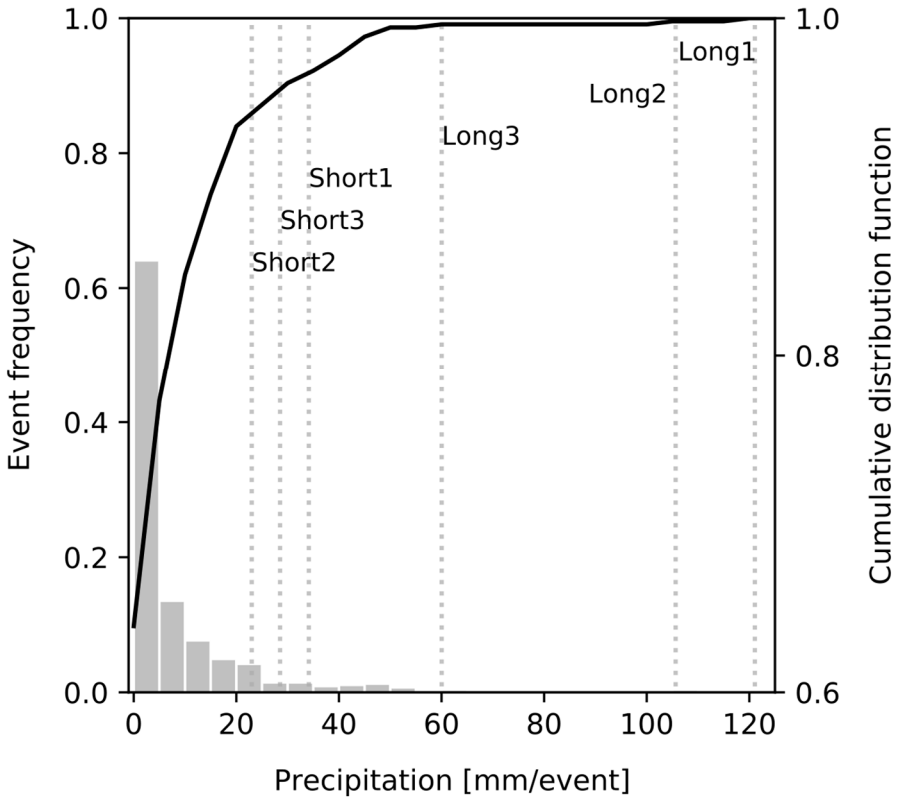

Figure A3. Classification of the selected most extreme three short-duration and three long-duration events within our study time frame over the extended summer months (May to September) in 2009–2014.

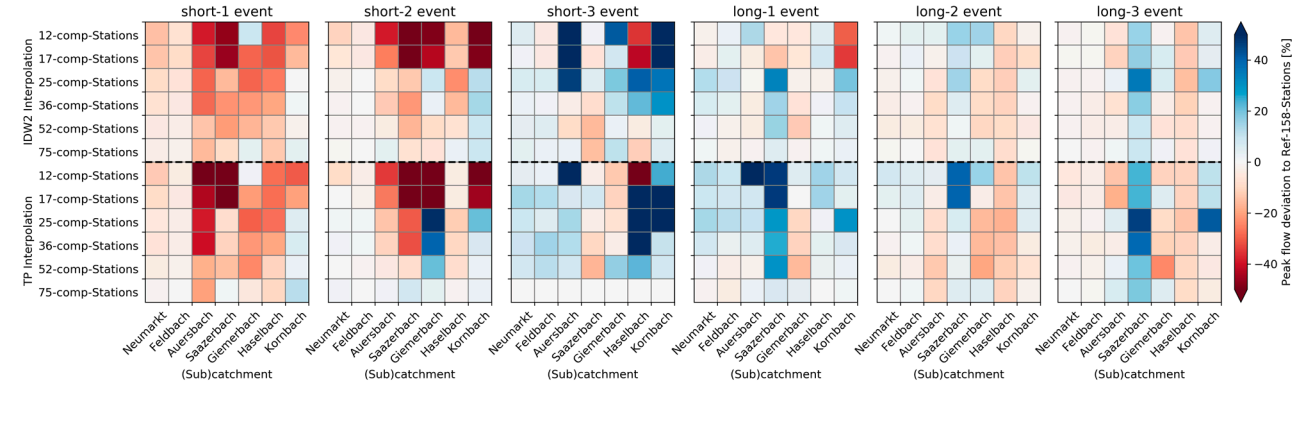

(**a**)

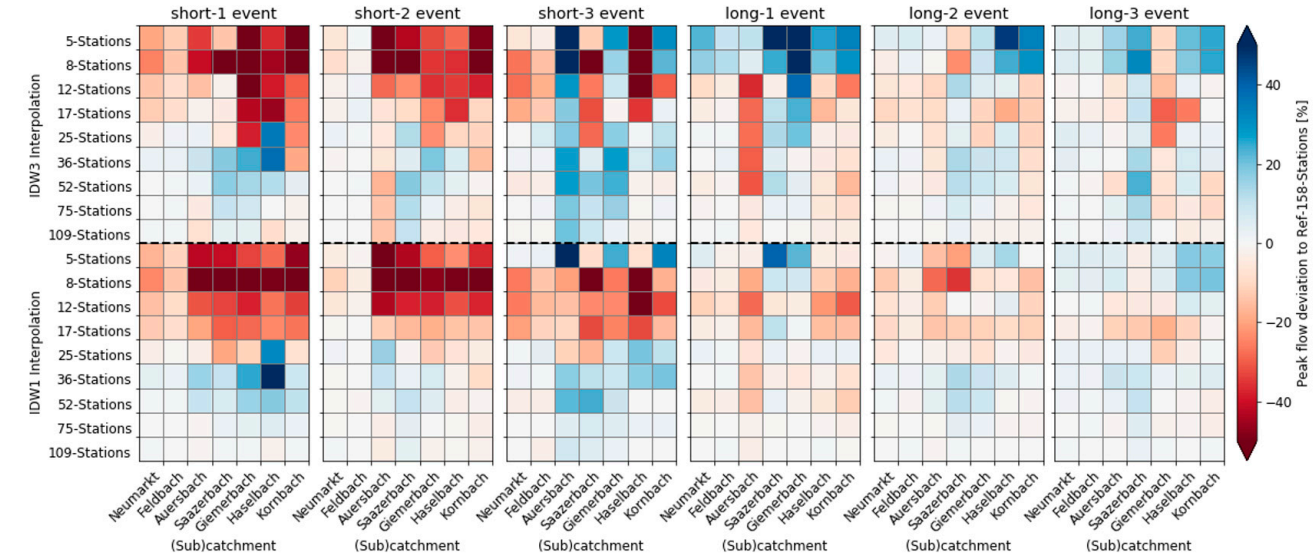

(**b**)

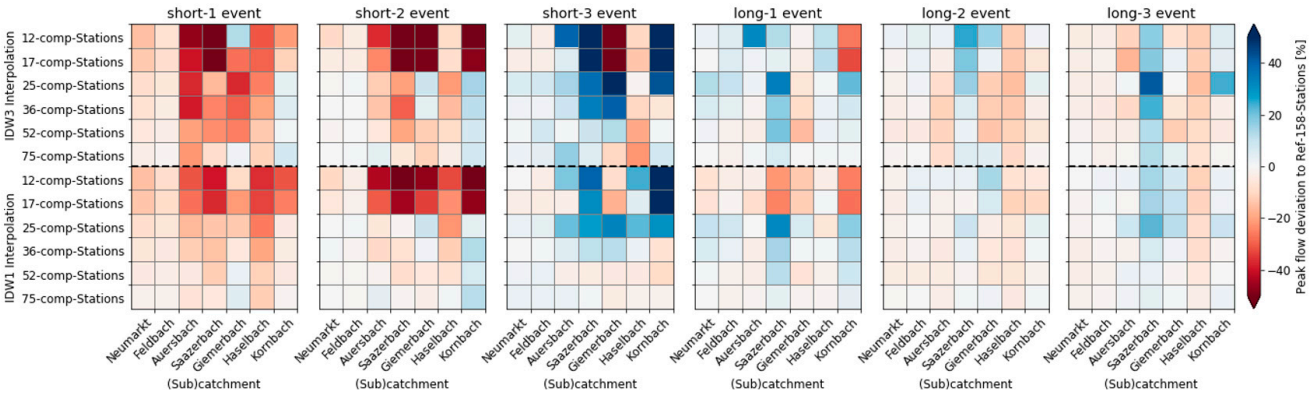

(**c**)

Figure A4. Complementary to Figure 7. Peak flow deviation to Ref-158-Stations case as a grid-cell plot with each cell indicating the magnitude of the deviation on a color-scale, for the cases of all six events (one event per panel), all (sub)catchments (columns per panel), the four interpolation schemes inverse distance weighting with power of 2 (IDW2), power of 3 (IDW3), power of 1 (IDW1), and Thiessen polygons (TP)) (stacked subpanels per panel), and all subnetwork cases (rows per subpanel). (**a**) depicts the results of the complementary subnetwork of IDW2 and TP interpolation; (**b**) the results for the primary subnetworks for IDW3 and IDW1; (**c**) the ones of the complementary subnetworks (IDW3 and IDW1) analyzed in this study.

References

1. Kharin, V.V.; Zwiers, F.W.; Zhang, X.; Hegerl, G.C. Changes in Temperature and Precipitation Extremes in the IPCC Ensemble of Global Coupled Model Simulations. *J. Clim.* **2007**, *20*, 1419–1444, doi:10.1175/JCLI4066.1.
2. Chen, H.; Sun, J.; Chen, X.; Zhou, W. CGCM projections of heavy rainfall events in China. *Int. J. Climatol.* **2012**, *32*, 441–450, doi:10.1002/joc.2278.
3. Fischer, E.M.; Knutti, R. Observed heavy precipitation increase confirms theory and early models. *Nat. Clim. Chang.* **2016**, *6*, 986–991, doi:10.1038/nclimate3110.
4. Prein, A.F.; Rasmussen, R.M.; Ikeda, K.; Liu, C.; Clark, M.P.; Holland, G.J. The future intensification of hourly precipitation extremes. *Nat. Clim. Chang.* **2016**, *7*, 48–52, doi:10.1038/nclimate3168.
5. Bárdossy, A.; Das, T. Influence of rainfall observation network on model calibration and application. *Hydrol. Earth Syst. Sci.* **2008**, *12*, 77–89, doi:10.5194/hess-12-77-2008.
6. Zeng, Q.; Chen, H.; Xu, C.-Y.; Jie, M.-X.; Chen, J.; Guo, S.-L.; Liu, J. The effect of rain gauge density and distribution on runoff simulation using a lumped hydrological modelling approach. *J. Hydrol.* **2018**, *563*, 106–122, doi:10.1016/J.JHYDROL.2018.05.058.
7. Gilewski, P.; Nawalany, M. Inter-Comparison of Rain-Gauge, Radar, and Satellite (IMERG GPM) Precipitation Estimates Performance for Rainfall-Runoff Modeling in a Mountainous Catchment in Poland. *Water* **2018**, *10*, 1665, doi:10.3390/w10111665.
8. St-Hilaire, A.; Ouarda, T.B.M.J.; Lachance, M.; Bobée, B.; Gaudet, J.; Gignac, C. Assessment of the impact of meteorological network density on the estimation of basin precipitation and runoff: A case study. *Hydrol. Process.* **2003**, *17*, 3561–3580, doi:10.1002/hyp.1350.
9. Maier, R.; Krebs, G.; Pichler, M.; Muschalla, D.; Gruber, G. Spatial Rainfall Variability in Urban Environments—High-Density Precipitation Measurements on a City-Scale. *Water* **2020**, *12*, doi:10.3390/w12041157.
10. McMillan, H. k. K. Effect of spatial variability and seasonality in soil moisture on drainage thresholds and fluxes in a conceptual hydrological model. *Hydrol. Process.* **2012**, *26*, 2838–2844, doi:10.1002/hyp.9396.
11. Goodrich, D.C.; Faurès, J.-M.; Woolhiser, D.A.; Lane, L.J.; Sorooshian, S. Measurement and analysis of small-scale convective storm rainfall variability. *J. Hydrol.* **1995**, *173*, 283–308, doi:10.1016/0022-1694(95)02703-R.
12. Huang, Y.; Bárdossy, A.; Zhang, K. Sensitivity of hydrological models to temporal and spatial resolutions of rainfall data. *Hydrol. Earth Syst. Sci.* **2019**, *23*, 2647–2663, doi:10.5194/hess-23-2647-2019.
13. O, S.; Foelsche, U. Assessment of spatial uncertainty of heavy rainfall at catchment scale using a dense gauge network. *Hydrol. Earth Syst. Sci.* **2019**, *23*, 2863–2875, doi:10.5194/hess-23-2863-2019.
14. Kidd, C.; Huffman, G. Review Global precipitation measurement. *Meteorol. Appl.* **2011**, *18*, 334–353, doi:10.1002/met.284.
15. Sun, X.; Mein, R.G.; Keenan, T.D.; Elliott, J.F. Flood estimation using radar and raingauge data. *J. Hydrol.* **2000**, *239*, 4–18, doi:10.1016/S0022-1694(00)00350-4.
16. Tetzlaff, D.; Uhlenbrook, S. Significance of spatial variability in precipitation for process-oriented modelling: Results from two nested catchments using radar and ground station data. *Hydrol. Earth Syst. Sci.* **2005**, *9*, 29–41, doi:10.5194/hess-9-29-2005.
17. Tian, Y.; Peters-Lidard, C.D. A global map of uncertainties in satellite-based precipitation measurements. *Geophys. Res. Lett.* **2010**, *37*, L24407, doi:10.1029/2010GL046008.
18. Kirstetter, P.-E.; Hong, Y.; Gourley, J.J.; Chen, S.; Flamig, Z.; Zhang, J.; Schwaller, M.; Petersen, W.; Amitai, E. Toward a Framework for Systematic Error Modeling of Spaceborne Precipitation Radar with NOAA/NSSL Ground Radar–Based National Mosaic QPE. *J. Hydrometeorol.* **2012**, *13*, 1285–1300, doi:10.1175/JHM-D-11-0139.1.
19. O, S.; Foelsche, U.; Kirchengast, G.; Fuchsberger, J.; Tan, J.; Petersen, W.A. Evaluation of GPM IMERG Early, Late, and Final rainfall estimates using WegenerNet gauge data in southeastern Austria. *Hydrol. Earth Syst. Sci.* **2017**, *21*, 6559–6572, doi:10.5194/hess-21-6559-2017.
20. Lasser, M.; O, S.; Foelsche, U. Evaluation of GPM-DPR precipitation estimates with WegenerNet gauge data. *Atmos. Meas. Tech.* **2019**, *12*, 5055–5070, doi:10.5194/amt-12-5055-2019.
21. Ghaemi, E.; Foelsche, U.; Kann, A.; Fuchsberger, J. Evaluation of INCA precipitation analysis using a very dense rain gauge network in southeast Austria. *Hydrol. Earth Syst. Sci. Discuss.* **2021**, in review, doi:10.5194/hess-2021-34.
22. Lopez, M.G.; Wennerström, H.; Nordén, L.; Seibert, J. Location and density of rain gauges for the estimation of spatial varying precipitation. *Geogr. Ann. Ser. A Phys. Geogr.* **2015**, *97*, 167–179, doi:10.1111/geoa.12094.
23. Goovaerts, P. Geostatistical approaches for incorporating elevation into the spatial interpolation of rainfall. *J. Hydrol.* **2000**, *228*, 113–129, doi:10.1016/S0022-1694(00)00144-X.
24. Obled, C.; Wendling, J.; Beven, K.J. The sensitivity of hydrological models to spatial rainfall patterns: An evaluation using observed data. *J. Hydrol.* **1994**, *159*, 305–333, doi:10.1111/j.1474-919X.1892.tb00320.x.
25. Dong, X.; Dohmen-Janssen, C.M.; Booij, M.J. Appropriate Spatial Sampling of Rainfall or Flow Simulation. *Hydrol. Sci. J.* **2005**, *50*, 279–298, doi:10.1623/hysj.50.2.279.61801.
26. Meselhe, E.A.; Habib, E.H.; Oche, O.C.; Gautam, S. Sensitivity of conceptual and physically based hydrologic models to temporal and spatial rainfall sampling. *J. Hydrol. Eng.* **2009**, *14*, 711–720, doi:10.1061/(ASCE)1084-0699(2009)14:7(711).
27. Xu, H.; Xu, C.-Y.; Chen, H.; Zhang, Z.; Li, L. Assessing the influence of rain gauge density and distribution on hydrological model performance in a humid region of China. *J. Hydrol.* **2013**, *505*, 1–12, doi:10.1016/J.JHYDROL.2013.09.004.
28. Zhang, X.; Srinivasan, R. Gis-based spatial precipitation estimation: A comparison of geostatistical approaches. *J. Am. Water Resour. Assoc.* **2009**, *45*, 894–906, doi:10.1111/j.1752-1688.2009.00335.x.

29. Ly, S.; Charles, C.; Degré, A.; Sarann Ly, C.C.A.D. Different methods for spatial interpolation of rainfall data for operational hydrology and hydrological modeling at watershed scale. A review. *Biotechnol. Agron. Société Environ.* **2013**, *17*, 392–406.
30. Szcześniak, M.; Piniewski, M. Improvement of Hydrological Simulations by Applying Daily Precipitation Interpolation Schemes in Meso-Scale Catchments. *Water* **2015**, *7*, 747–779, doi:10.3390/w7020747.
31. Andréassian, V.; Perrin, C.; Michel, C.; Usart-Sanchez, I.; Lavabre, J. Impact of imperfect rainfall knowledge on the efficiency and the parameters of watershed models. *J. Hydrol.* **2001**, *250*, 206–223, doi:10.1016/S0022-1694(01)00437-1.
32. Kobold, M.; Brilly, M. The use of HBV model for flash flood forecasting. *Nat. Hazards Earth Syst. Sci.* **2006**, *6*, 407–417, doi:10.5194/nhess-6-407-2006.
33. Verworn, A.; Haberlandt, U. Spatial interpolation of hourly rainfall-effect of additional information, variogram inference and storm properties. *Hydrol. Earth Syst. Sci.* **2011**, *15*, 569–584, doi:10.5194/hess-15-569-2011.
34. Schwarzak, S.; Hänsel, S.; Matschullat, J. Projected changes in extreme precipitation characteristics for Central Eastern Germany (21st century, model-based analysis). *Int. J. Climatol.* **2015**, *35*, 2724–2734, doi:10.1002/joc.4166.
35. Breinl, K.; Müller-Thomy, H.; Blöschl, G. Space–Time Characteristics of Areal Reduction Factors and Rainfall Processes. *J. Hydrometeorol.* **2020**, *21*, 671–689, doi:10.1175/JHM-D-19-0228.1.
36. Kirchengast, G.; Kabas, T.; Leuprecht, A.; Bichler, C.; Truhetz, H. WegenerNet: A Pioneering High-Resolution Network for Monitoring Weather and Climate. *Bull. Am. Meteorol. Soc.* **2014**, *95*, 227–242, doi:10.1175/BAMS-D-11-00161.1.
37. Chen, F.W.; Liu, C.W. Estimation of the spatial rainfall distribution using inverse distance weighting (IDW) in the middle of Taiwan. *Paddy Water Environ.* **2012**, *10*, 209–222, doi:10.1007/s10333-012-0319-1.
38. Gilewski, P. Impact of the Grid Resolution and Deterministic Interpolation of Precipitation on Rainfall-Runoff Modeling in a Sparsely Gauged Mountainous Catchment. *Water* **2021**, *13*, 230, doi:10.3390/w13020230.
39. Kurtzman, D.; Navon, S.; Morin, E. Improving interpolation of daily precipitation for hydrologic modelling: Spatial patterns of preferred interpolators. *Hydrol. Process.* **2009**, *23*, 3281–3291, doi:10.1002/hyp.7442.
40. Dirks, K.N.; Hay, J.E.; Stow, C.D.; Harris, D. High-resolution studies of rainfall on Norfolk Island Part II: Interpolation of rainfall data. *J. Hydrol.* **1998**, *208*, 187–193, doi:10.1016/S0022-1694(98)00155-3.
41. Schroeer, K.; Kirchengast, G. Sensitivity of extreme precipitation to temperature: The variability of scaling factors from a regional to local perspective. *Clim. Dyn.* **2018**, *50*, 3981–3994, doi:10.1007/s00382-017-3857-9.
42. Schulla, J. Hydrologische Modellierung von Flussgebieten zur Abschätzung der Folgen von Klimaänderungen. Ph.D. Thesis, ETH Zurich, Zurich, Switzerland, 1997.
43. Gervais, M.; Tremblay, L.B.; Gyakum, J.R.; Atallah, E. Representing Extremes in a Daily Gridded Precipitation Analysis over the United States: Impacts of Station Density, Resolution, and Gridding Methods. *J. Clim.* **2014**, *27*, 5201–5218, doi:10.1175/JCLI-D-13-00319.1.
44. Avila, F.B.; Dong, S.; Menang, K.P.; Rajczak, J.; Renom, M.; Donat, M.G.; Alexander, L.V. Systematic investigation of gridding-related scaling effects on annual statistics of daily temperature and precipitation maxima: A case study for south-east Australia. *Weather Clim. Extrem.* **2015**, *9*, 6–16, doi:10.1016/j.wace.2015.06.003.
45. Herrera, S.; Kotlarski, S.; Soares, P.M.M.M.; Cardoso, R.M.; Jaczewski, A.; Gutiérrez, J.M.; Maraun, D. Uncertainty in gridded precipitation products: Influence of station density, interpolation method and grid resolution. *Int. J. Climatol.* **2018**, *39*, 3717–3729, doi:10.1002/joc.5878.
46. Hohmann, C.; Kirchengast, G.; Birk, S. Alpine foreland running drier? Sensitivity of a drought vulnerable catchment to changes in climate, land use, and water management. *Clim. Change* **2018**, *147*, 179–193, doi:10.1007/s10584-017-2121-y.
47. O, S.; Foelsche, U.; Kirchengast, G.; Fuchsberger, J. Validation and correction of rainfall data from the WegenerNet high density network in southeast Austria. *J. Hydrol.* **2018**, *556*, 1110–1122, doi:10.1016/j.jhydrol.2016.11.049.
48. Haiden, T.; Kann, A.; Wittmann, C.; Pistotnik, G.; Bica, B.; Gruber, C. The integrated nowcasting through comprehensive analysis (INCA) system and its validation over the Eastern Alpine region. *Weather Forecast.* **2011**, *26*, 166–183, doi:10.1175/2010WAF2222451.1.
49. Klebinder, K.; Sotier, B.; Lechner, V.; Strauss, P. *Hydrologische und hydropedologische Kenndaten Raabgebiet und Region Südoststeiermark*; Department of Natural Hazards, Austrian Research Center for Forests (BFW): Innsbruck, Austria, 2017.
50. Fuchsberger, J.; Kirchengast, G.; Bichler, C.; Leuprecht, A.; Kabas, T. WegenerNet climate station network Level 2 data version 7.1 (2007–2020). *Wegener Center for Climate and Global Change*; University of Graz: Graz, Austria, **2021**. doi:10.25364/WEGC/WPS7.1:2021.1.
51. Krammer, C.; Klebinder, K.; Eder, A.; Sotier, B.; Strauss, P.; Bauer, T. HYDROBOD: Obtaining a GIS-based hydrological soil database and a runoff coefficient calculator for Lower Austria. *Forum Geogr.* **2016**, *XV*, 100–104, doi:10.5775/fg.2016.123.s.
52. Bürger, G.; Schulla, J.; Werner, A.T. Estimates of future flow, including extremes, of the Columbia River headwaters. *Water Resour. Res.* **2011**, *47*, 1–18, doi:10.1029/2010WR009716.
53. Gädeke, A.; Hölzel, H.; Koch, H.; Pohle, I.; Grünewald, U. Analysis of uncertainties in the hydrological response of a model-based climate change impact assessment in a subcatchment of the Spree River, Germany. *Hydrol. Process.* **2014**, *28*, 3978–3998, doi:10.1002/hyp.9933.
54. Alaoui, A.; Willimann, E.; Jasper, K.; Felder, G.; Herger, F.; Magnusson, J.; Weingartner, R. Modelling the effects of land use and climate changes on hydrology in the Ursern Valley, Switzerland. *Hydrol. Process.* **2014**, *28*, 3602–3614, doi:10.1002/hyp.9895.
55. Yira, Y.; Diekkrüger, B.; Steup, G.; Bossa, A.Y. Modeling land use change impacts on water resources in a tropical West African catchment (Dano, Burkina Faso). *J. Hydrol.* **2016**, *537*, 187–199, doi:10.1016/j.jhydrol.2016.03.052.

56. Schulla, J. Model Description WaSiM (Water Balance Simulation Model); Hydrology Software Consulting J. Schulla, Zurich, Switzerland 2019, www.wasim.ch (accessed on 25 March 2021).
57. Monteith, J.L. Evaporation and environment. *Symp. Soc. Exp. Biol.* **1965**, *19*, 205–234.
58. van Genuchten, M.T. Closed-Form Equation for Predicting the Hydraulic Conductivity of Unsaturated Soils. *Soil Sci. Soc. Am. J.* **1980**, *44*, 892–898.
59. Nash, J.E.; Sutcliffe, J.V. River flow forecasting through conceptual models part I—A discussion of principles. *J. Hydrol.* **1970**, *10*, 282–290, doi:10.1016/0022-1694(70)90255-6.
60. Gupta, H.V.; Kling, H.; Yilmaz, K.K.; Martinez, G.F. Decomposition of the mean squared error and NSE performance criteria: Implications for improving hydrological modelling. *J. Hydrol.* **2009**, *377*, 80–91, doi:10.1016/j.jhydrol.2009.08.003.
61. Moriasi, D.N.; Arnold, J.G.; Van Liew, M.W.; Bingner, R.L.; Harmel, R.D.; Veith, T.L. Model evaluation guidelines for systematic quantification of accuracy in watershed simulations. *Trans. ASABE* **2007**, *50*, 885–900, doi:10.13031/2013.23153.
62. Watson, A.; Kralisch, S.; Künne, A.; Fink, M.; Miller, J. Impact of precipitation data density and duration on simulated flow dynamics and implications for ecohydrological modelling in semi-arid catchments in Southern Africa. *J. Hydrol.* **2020**, *590*, 125280, doi:10.1016/j.jhydrol.2020.125280.
63. Duan, Q.; Sorooshian, S.; Gupta, V.K. Optimal use of the SCE-UA global optimization method for calibrating watershed models. *J. Hydrol.* **1994**, *158*, 265–284, doi:10.1016/0022-1694(94)90057-4.
64. Schroeer, K.; Tye, M.R. Quantifying damage contributions from convective and stratiform weather types: How well do precipitation and discharge data indicate the risk? *J. Flood Risk Manag.* **2018**, doi:10.1111/jfr3.12491.
65. Dunkerley, D. Identifying individual rain events from pluviograph records: A review with analysis of data from an Australian dryland site. *Hydrol. Process.* **2008**, *22*, 5024–5036, doi:10.1002/hyp.7122.
66. Cheng, M.; Wang, Y.; Engel, B.; Zhang, W.; Peng, H.; Chen, X.; Xia, H.; Cheng, M.; Wang, Y.; Engel, B.; et al. Performance Assessment of Spatial Interpolation of Precipitation for Hydrological Process Simulation in the Three Gorges Basin. *Water* **2017**, *9*, 838, doi:10.3390/w9110838.
67. Syed, K.H.; Goodrich, D.C.; Myers, D.E.; Sorooshian, S. Spatial characteristics of thunderstorm rainfall fields and their relation to runoff. *J. Hydrol.* **2003**, *271*, 1–21, doi:10.1016/S0022-1694(02)00311-6.
68. Beven, K.J.; Hornberger, G.M. Assessing the Effect of Spatial Pattern of Precipitation in Modeling Stream Flow Hydrographs. *J. Am. Water Resour. Assoc.* **1982**, *18*, 823–829, doi:10.1111/j.1752-1688.1982.tb00078.x.
69. Fuchsberger, J.; Kirchengast, G.; Kabas, T. WegenerNet high-resolution weather and climate data from 2007 to 2020. *Earth Syst. Sci. Data* **2021**, *13*, 1307–1334, doi:10.5194/ essd-13-1307-2021.
70. Kabas, T. WegenerNet climate station network region Feldbach: Experimental setup and high- resolution data for weather and climate research (in German). *Wegener Cent. Sci. Rep.* **2012**, *47*, 177.
71. Lamptey, B.L. Comparison of gridded multisatellite rainfall estimates with gridded gauge rainfall over West Africa. *J. Appl. Meteorol. Climatol.* **2008**, *47*, 185–205, doi:10.1175/2007JAMC1586.1.
72. Schroeer, K.; Kirchengast, G.; O, S. Strong Dependence of Extreme Convective Precipitation Intensities on Gauge Network Density. *Geophys. Res. Lett.* **2018**, *45*, 8253–8263, doi:10.1029/2018GL077994.